

Synthetic horizontal branch morphology for different metallicities and ages under tidally enhanced stellar wind

Z. Lei^{1,2,3}, F. Zhang^{1,2}, H. Ge^{1,2}, and Z. Han^{1,2}

¹ National Astronomical Observatories/Yunnan Observatory, the Chinese Academy of Sciences, KunMing 650011, China

e-mail: lzx2008@ynao.ac.cn

² Key Laboratory for the Structure and Evolution of Celestial Objects, the Chinese Academy of Sciences, Kunming 650011, China

³ University of the Chinese Academy of Sciences, Beijing 100049, China

Received ; accepted

ABSTRACT

Context. It is believed that some other parameters, except for metallicity (the first parameter), are needed to explain the horizontal branch (HB) morphology of globular clusters (GCs). Furthermore, these parameters are considered to be correlated with the mass loss of the red giant branch (RGB) stars. Unfortunately, the physics of mass loss on the RGB is poorly understood at present. In our previous work, we proposed that tidally enhanced stellar wind during binary evolution may affect the HB morphology by enhancing the mass loss of the red giant primary and that we can reproduce the basic morphology of HB in GCs.

Aims. We did not consider the effects of other important parameters (e.g., metallicity and age) in our final results there. As a further study, we now investigate the effects of metallicity and age on HB morphology by considering tidally enhanced stellar winds during binary evolution.

Methods. We incorporated the tidally enhanced-stellar-wind model of Tout & Eggleton into Eggleton's stellar evolution code to study the binary evolution. A group of binary system samples were generated by Monte Carlo simulations. The position of each sample star in a color-magnitude diagram was obtained by transforming temperature and luminosity into $B - V$ color and absolute magnitude. To study the effects of metallicity and age on our final results, we conducted two sets of model calculations: (i) for a fixed age, we used three metallicities, namely $Z=0.0001$, 0.001 and 0.02 . (ii) for a fixed metallicity, $Z = 0.001$, we used five ages in our model calculations: 14, 13, 12, 10, 7 Gyr.

Results. We found that HB morphology of GCs becomes bluer with decreasing metallicity, and old GCs present bluer HB morphology than young ones. These results are consistent with previous work. Although the envelope-mass distributions of zero-age HB stars produced by tidally enhanced stellar wind are similar for different metallicities, the synthetic HB under tidally enhanced stellar wind for $Z=0.02$ presented a distinct gap between red and blue HB. However, this feature was not seen clearly in the synthetic HB for $Z=0.001$ and 0.0001 . We also found that binary fractions may make HB morphology become bluer, and we discuss the results with recent observations.

Key words. Clusters: globular clusters - star: horizontal branch - star: stellar evolution

1. Introduction

The color distribution of horizontal branch (HB) stars in the color-magnitude diagram (CMD) of globular clusters (GCs), which is defined as HB morphology, is a longstanding problem in stellar evolution. Although the most important factor affecting HB morphology is identified as the metallicity (called the first parameter, Sandage & Wallerstein 1960), other parameters are also believed to play an important role in this problem. These parameters are called the second parameter (2P). However, the nature of the 2P is still unknown. Many 2P candidates have been proposed in the past five decades (for a recent review see Catelan 2009; also see Lei et al. 2013; here after Paper I), but none of them can explain the whole HB morphologies in GCs. Recently, some researchers have suggested that, except for metallicity, age may be the main global parameter affecting HB morphology in GCs, while some other parameters are needed as the third parameter, such as helium abundance and central density (Gratton et al. 2010; Dotter et al. 2010). Moreover, the second parameter problem is considered to be correlated with multiple populations discovered in GCs (Piotto et al. 2007, 2012; Carretta et al. 2010; Gratton, Carretta & Bragaglia, 2012).

Mass loss on the red giant branch (RGB) is a very important process in understanding the 2P problem in GCs (Catelan 2009), since the color distribution of HB stars in CMD depends on their envelope masses, while the envelope mass is determined by the mass loss on the RGB. Unfortunately, the physics of mass loss on the RGB is poorly known at present (Willson 2000; Dupree et al. 2009). Thus, in order to reproduce the color distribution of HB stars in the CMD of GCs, most of the 2P candidates need to assume a mass-loss dispersion on the RGB (e.g., Gaussian distribution of mass with a mass dispersion for HB stars; Lee, Yoon & Lee 2000; Lee et al. 1994; D'Antona & Caloi, 2004; Percival & Salaris 2011). However, the assumption of mass-loss dispersion is arbitrary and has no any physical justification.

In our previous work (see Paper I), we proposed that tidally enhanced stellar wind during binary evolution may affect the HB morphology in GCs by enhancing the mass loss of the red giant primary. In a red giant binary system, the stellar wind of the red giant primary may be tidally enhanced by the secondary. The exact mass loss of the primary stars on the RGB depends on the initial binary orbital period. Therefore different initial binary orbital periods lead to different mass loss of the primary on the RGB. After the ignition of helium in their cores, the primary stars are located in different positions of the HB. In Paper I, under consideration of tidally enhanced stellar wind and without any additional assumptions of mass-loss dispersion on the RGB, we can reproduce the basic HB morphology of GCs, in which red, blue, and extreme HB are all populated. However, we do not know exactly how other important parameters (e.g., metallicity and age) affect our results obtained in Paper I. As further study, in this paper, using the same method as described in Paper I, we study the effects on HB morphology for different metallicities and ages by considering the tidally enhanced stellar wind during binary evolution.

The structure of this paper is as follows. In Section 2, we introduce the method and code used in this paper. Our results are given in Section 3. A discussion and conclusions are given in Section 4 and Section 5, respectively.

2. Method and code

As described in Paper I, in this work, we also incorporate tidally enhanced stellar wind during binary evolution (see Sect 2.2) into Eggleton’s stellar evolution code (see Sect 2.1) to calculate the stellar mass and the helium core mass of the primary star at the helium flash (hereafter M_{HF} and $M_{\text{c,HF}}$, respectively). Then, M_{HF} , $M_{\text{c,HF}}$, and a lifetime spent on the HB are used to obtain the exact position of the primary star (e.g., effective temperature and luminosity) on the HB in the Hertzsprung-Russell (H-R) diagram by interpolating among constructed HB evolutionary tracks. All the HB evolutionary tracks are constructed using modules for experiments in stellar astrophysics (MESA; Paxton et al. 2011; see Paper I for details). Finally, we transform the effective temperature and luminosity of each HB star into $B - V$ colors and absolute magnitudes, M_V , to obtain the synthetic HB morphology in CMD. All these processes are carried out for different metallicities and ages to investigate the effects of these two parameters on the final results.

2.1. Stellar evolution code

Eggleton’s stellar evolution code was developed in the early 1970s (Eggleton 1971, 1972, 1973). This code has been updated with the latest input physics over the past four decades (Han et al. 1994; Pols et al. 1995, 1998). Now, this code is being applied extensively in the field of stellar evolution. In our calculations, the ratio of mixing length to local pressure scale height, $\alpha = l/H_P$, is set to 2.0. The convective overshooting parameter, δ_{ov} , is set to 0.12 (Pols et al. 1997). The opacity used in our calculations was compiled by Chen & Tout (2007). We obtain the initial hydrogen mass fraction, X , by $X = 0.76 - 3Z$, where Z is the metallicity (Pols et al. 1998).

2.2. Tidally enhanced stellar wind

We use the same equation as in Paper I to describe the tidally enhanced stellar wind during binary evolution,

$$\dot{M} = -\eta 4 \times 10^{-13} (RL/M) \{1 + B_w \times \min[(R/R_L)^6, 1/2^6]\}, \quad (1)$$

where η is the Reimers mass-loss efficiency, R_L is the radius of the Roche lobe, B_w is the tidal enhancement efficiency, and R, L, M are in solar units. This form of stellar wind was first suggested by Tout & Eggleton (1988) to explain the mass inversion phenomenon found in some RS CVn binary systems (see Paper I for detail). We incorporate equation (1) into Eggleton’s stellar evolution code to calculate M_{HF} and $M_{\text{c,HF}}$ of the primary star.

From our previous result in Paper I, the HB morphology is not very sensitive to the tidal enhancement parameter, B_w . For this reason, B_w is set to 10000 (e.g., the typical value used in Tout & Eggleton 1988) in all sets of calculations in this paper. Reimers mass-loss efficiency (Reimers 1975), η , is set to 0.45 (see the discussion in Section 4.2). To study the effects of metallicity and age on the HB morphology by considering tidally enhanced stellar wind, we carry out two sets of calculations: (i) for a fixed age of 13 Gyr, we use three different metallicities, namely $Z=0.0001$, 0.001, and 0.02. For these three metallicities, the stellar mass of the primary at zero-age main sequence (hereafter M_{ZAMS}) are 0.80, 0.83 and $0.98M_{\odot}$ respectively. (ii) For a fixed metallicity of GCs, $Z=0.001$, we use five M_{ZAMS} in our model calculations, namely 0.80, 0.83, 0.85, 0.89, and $0.97M_{\odot}$. These five masses correspond to cluster ages of 14, 13, 12, 10, and 7 Gyr, respectively. The

Table 1. Information for the two sets of calculations in this paper.

	Z	$M_{\text{ZAMS}}(M_{\odot})$	age (Gyr)
set(i)	0.0001	0.80	13
	0.001	0.83	13
	0.02	0.98	13
set(ii)	0.001	0.80	14
	0.001	0.83	13
	0.001	0.85	12
	0.001	0.89	10
	0.001	0.97	7

detailed information for the two sets of calculations are shown in Table 1. The columns from left to right provide the metallicity, M_{ZAMS} , and the age of the primary star at helium flash, respectively. The results of the two sets of calculations are given in Tables 2 and 3 (see Section 3.1).

The mass ratio of primary to secondary is set to 1.6 (We used different mass ratios of primary to secondary in Paper I, but it has little influence on our results.) We assume that the mass accreted by the secondary from the stellar wind is retained in the binary system, and the angular momentum that leaves the binary system due to the stellar wind is attributed to the primary star.

2.3. Initial binary samples

To obtain the synthetic HB morphology in CMD, we generate several groups of binary systems, in which the metallicity and M_{ZAMS} of the primary stars correspond to the values given in Table 1. The mass ratio of primary to secondary is set to 1.6 (see Section 2.2). The initial orbital periods of all binary systems are produced by Monte Carlo simulations. The distribution of separation in binary is constant in $\log a$ (a is the separation) and falls off smoothly at small separations,

$$a \cdot n(a) = \begin{cases} \alpha_{\text{sep}}(a/a_0)^m, & a \leq a_0, \\ \alpha_{\text{sep}}, & a_0 < a < a_1, \end{cases} \quad (2)$$

where $\alpha_{\text{sep}} \approx 0.07$, $a_0 = 10 R_{\odot}$, $a_1 = 5.75 \times 10^6 R_{\odot} = 0.13 \text{ pc}$ and $m \approx 1.2$. This distribution implies that the number of wide binaries per logarithmic interval are equal and about 50% of stellar systems have orbital periods less than 100 yr (Han et al. 2003).

3. Results

3.1. M_{HF} and $M_{\text{c,HF}}$ of the primary star for different metallicities and ages.

Table 2 shows the results of our model calculation for different metallicities, and it gives the M_{HF} , $M_{\text{c,HF}}$, and the envelope mass of the primary stars at the helium flash (M_{env}) with various initial binary orbital periods at a fixed age of 13 Gyr. The results in Table 2 correspond to the calculation of set (i) (see Section 2.2). Recall that B_{w} is set to 10^4 and η is set to 0.45. The mass ratio of primary-to-secondary, q , is set to be 1.6. The columns from left to right provide the initial orbital periods, M_{HF} , $M_{\text{c,HF}}$, and M_{env} , respectively.

For each metallicity, the first binary orbital period in Table 2 is a minimum period (e.g., $\log P/\text{day} = 3.126$ for $M_{\text{ZAMS}} = 0.8M_{\odot}$ at metallicity of $Z = 0.0001$), above which a helium flash could take place. For orbital periods shorter than this critical value¹, the primary stars experience too much mass loss on the RGB due to the tidally enhanced stellar wind, and fail to ignite helium in their cores. Therefore, these primary stars will not undergo the HB phase and evolve into helium white dwarf (WD) cooling curve directly. With the increase in binary orbital period, the amount of mass loss of the primary star on the RGB decreases for each metallicity. When the initial binary orbital period is long enough, the tidally enhanced stellar wind becomes unimportant and has little effect on the mass loss of red giant primary (One can see that the M_{env} of primary stars with $\log P/\text{day} = 3.55$ and $\log P/\text{day}=10.0$ for $M_{\text{ZAMS}} = 0.8M_{\odot}$ at the metallicity of $Z = 0.0001$ are nearly the same, which means that they experience nearly the same amount of mass loss on the RGB.) At this time, the primary star just loses its envelope mass through Reimers mass-loss law (Reimers 1975).

Similar to Table 2, Table 3 presents our model calculation results for different ages at metallicity of $Z=0.001$, which corresponds to the calculation of set (ii) (see Section 2.2).

3.2. Synthetic HB morphology in CMD for different metallicities

To obtain the position of each sample star on the HB in the H-R diagram (e.g., effective temperatures and luminosities), we need to know M_{HF} , $M_{\text{c,HF}}$, and the time spent on HB phase which means how long the HB star has been evolved from zero-age HB (ZAHB). The value of M_{HF} and $M_{\text{c,HF}}$ for each primary star in this set of calculation are obtained by interpolating with the results presented in Table 2. The time spent on the HB is generated by a uniform random number between 0 and the HB lifetime, τ_{HB} (Rood 1973; Lee et al. 1990; Dalessandro et al. 2011). Here, τ_{HB} is set to be the lifetime of HB star with the lowest stellar mass among the constructed HB evolutionary tracks, which means that this star has the longest lifetime on the HB. Therefore, some of HB stars are given a time longer than their lifetimes on the HB, and these stars are considered to evolve into the next evolutionary phase (e.g., AGB or WD). This process is equivalent to the scenario that stars enter the HB from the RGB at a constant rate (see Lee et al. 1990). We use M_{HF} , $M_{\text{c,HF}}$, and the time spent on HB phase to obtain the exact position of each primary star on HB in the H-R diagram by interpolating among constructed HB evolutionary tracks. After that, we transform the temperature and luminosity of each HB star into $B - V$ color and absolute magnitude, M_V , using the Basel stellar spectra library (Lejeune et al. 1997, 1998). Finally, we obtain the synthetic HB in CMD.

Figure.1 shows the synthetic HB for three different metallicities under the tidally enhanced stellar wind. The metallicities from the top to bottom panels in Fig.1 are $Z=0.02$, 0.001 , and 0.0001 , respectively. The corresponding M_{ZAMS} are 0.98 , 0.83 , and $0.80M_{\odot}$. In the top panel of Fig.1, the synthetic HB has a high metallicity of $Z=0.02$. Most of HB stars in this panel locate in red HB (e.g., 95%), while stars in blue and extreme HB are just about 5%. One can see clearly in this panel that there is a distinct gap between red and blue HB, and a few of HB stars are located in

¹ If the binary orbital period is short enough to make the the primary star fill its Roche lobe, then a Roche lobe overflow (RLOF) or a common envelope (CE) will begin in this binary system, but this is beyond the scope of present work.

Table 2. M_{HF} , $M_{\text{c,HF}}$, and M_{env} of the primary with various initial binary orbital periods for different metallicities at a fixed age of 13 Gyr. Here, $B_{\text{w}} = 10000$, $\eta = 0.45$, $q = 1.6$.

$\log P/\text{day}$	$M_{\text{HF}}(M_{\odot})$	$M_{\text{c,HF}}(M_{\odot})$	$M_{\text{env}}(M_{\odot})$
<hr/>			
Z=0.0001, $M_{\text{ZAMS}} = 0.80 M_{\odot}$, age=13 Gyr			
3.1260	0.4869	0.4854	0.0015
3.1500	0.4904	0.4890	0.0014
3.2000	0.4976	0.4964	0.0012
3.2500	0.5047	0.5018	0.0029
3.3000	0.5328	0.5024	0.0304
3.3500	0.5688	0.5022	0.0666
3.4000	0.5932	0.5021	0.0911
3.4500	0.6088	0.5020	0.1068
3.5000	0.6186	0.5019	0.1167
3.5500	0.6247	0.5018	0.1229
10.000	0.6351	0.5017	0.1334
<hr/>			
Z=0.001, $M_{\text{ZAMS}} = 0.83 M_{\odot}$, age=13 Gyr			
3.2590	0.4725	0.4714	0.0011
3.3000	0.4783	0.4774	0.0009
3.3500	0.4854	0.4845	0.0009
3.4000	0.4926	0.4895	0.0031
3.4500	0.5309	0.4893	0.0416
3.5000	0.5677	0.4892	0.0785
3.5500	0.5935	0.4891	0.1044
3.6000	0.6103	0.4890	0.1213
3.6500	0.6208	0.4889	0.1319
10.000	0.6386	0.4887	0.1499
<hr/>			
Z=0.02, $M_{\text{ZAMS}} = 0.98 M_{\odot}$, age=13 Gyr			
3.5500	0.4504	0.4496	0.0008
3.6000	0.4571	0.4563	0.0008
3.7000	0.4709	0.4699	0.0010
3.7500	0.5171	0.4703	0.0468
3.8000	0.5910	0.4703	0.1207
3.8500	0.6491	0.4702	0.1789
3.9000	0.6853	0.4701	0.2152
3.9500	0.7072	0.4700	0.2372
4.0000	0.7206	0.4699	0.2507
4.5000	0.7421	0.4698	0.2723
10.000	0.7423	0.4698	0.2725
<hr/>			

the RR Lyrae instability strip. However, this bimodal HB morphology is not presented clearly in the other two panels of Fig.1. We discuss this result in Section 4.1. For the whole figure, with the metallicity decreasing from the top to bottom panels, more and more HB stars settle on blue and extreme HB. For the extreme case, in the bottom panel of Fig.1, which has the lowest metallicity of $Z=0.0001$ in our calculations, all HB stars are located in the region that is bluer than the RR Lyrae instability strip, with no red HB stars and RR Lyrae stars are produced. Figure.1 shows the typical effect of metallicity (the first parameter) on HB morphology in GCs, which is that metal-poor GCs present bluer HB morphology than the metal-rich ones. This is because the metal-poor GCs have a lower stellar mass than the metal-rich ones at the tip of RGB for a fixed cluster age. As a result, assuming that the mass-loss law on the RGB is the same, it is much easier for the metal-poor stars

Table 3. M_{HF} , $M_{\text{c,HF}}$, and M_{env} of the primary with various initial binary orbital periods for different ages at $Z = 0.001$. Here, $B_w = 10000$, $\eta = 0.45$, $q = 1.6$.

$\log P/\text{day}$	$M_{\text{HF}}(M_{\odot})$	$M_{\text{c,HF}}(M_{\odot})$	$M_{\text{env}}(M_{\odot})$
<hr/>			
Z=0.001,	$M_{\text{ZAMS}} = 0.80 M_{\odot}$,	age=14 Gyr	
3.2980	0.4734	0.4724	0.0010
3.3600	0.4817	0.4808	0.0009
3.4200	0.4894	0.4884	0.0010
3.4500	0.4933	0.4902	0.0031
3.5000	0.5210	0.4900	0.0310
3.5500	0.5463	0.4899	0.0564
3.6000	0.5641	0.4898	0.0743
3.6500	0.5758	0.4897	0.0861
10.000	0.5959	0.4896	0.1063
<hr/>			
Z=0.001,	$M_{\text{ZAMS}} = 0.83 M_{\odot}$,	age=13 Gyr	
3.2590	0.4725	0.4714	0.0011
3.3000	0.4783	0.4774	0.0009
3.3500	0.4854	0.4845	0.0009
3.4000	0.4926	0.4895	0.0031
3.4500	0.5309	0.4893	0.0416
3.5000	0.5677	0.4892	0.0785
3.5500	0.5935	0.4891	0.1044
3.6000	0.6103	0.4890	0.1213
3.6500	0.6208	0.4889	0.1319
10.000	0.6386	0.4887	0.1499
<hr/>			
Z=0.001,	$M_{\text{ZAMS}} = 0.85 M_{\odot}$,	age=12 Gyr	
3.2360	0.4719	0.4708	0.0011
3.3000	0.4813	0.4803	0.0010
3.3500	0.4886	0.4875	0.0011
3.4000	0.5146	0.4889	0.0257
3.4500	0.5637	0.4889	0.0748
3.5000	0.6008	0.4887	0.1121
3.5500	0.6251	0.4886	0.1365
3.6000	0.6405	0.4884	0.1521
3.6500	0.6502	0.4883	0.1619
10.000	0.6662	0.4883	0.1779
<hr/>			
Z=0.001,	$M_{\text{ZAMS}} = 0.89 M_{\odot}$,	age =10 Gyr	
3.1950	0.4708	0.4698	0.0010
3.2500	0.4792	0.4793	0.0009
3.3000	0.4869	0.4859	0.0010
3.3500	0.5162	0.4879	0.0283
3.4000	0.5832	0.4879	0.0953
3.4500	0.6338	0.4877	0.1461
3.5000	0.6665	0.4876	0.1789
3.5500	0.6868	0.4875	0.1993
3.6000	0.6993	0.4874	0.2119
3.6500	0.7071	0.4874	0.2197
10.000	0.7201	0.4873	0.2328
<hr/>			
Z=0.001,	$M_{\text{ZAMS}} = 0.97 M_{\odot}$,	age =7 Gyr	
3.1250	0.4687	0.4677	0.0010
3.2000	0.4808	0.4799	0.0009
3.2500	0.4894	0.4861	0.0033
3.3000	0.5827	0.4862	0.0965
3.3500	0.6741	0.4861	0.1880
3.4000	0.7319	0.4860	0.2459
3.4500	0.7669	0.4859	0.2810
3.5000	0.7882	0.4858	0.3024
3.5500	0.8013	0.4858	0.3155
3.6000	0.8094	0.4857	0.3237
10.000	0.8227	0.4856	0.3371

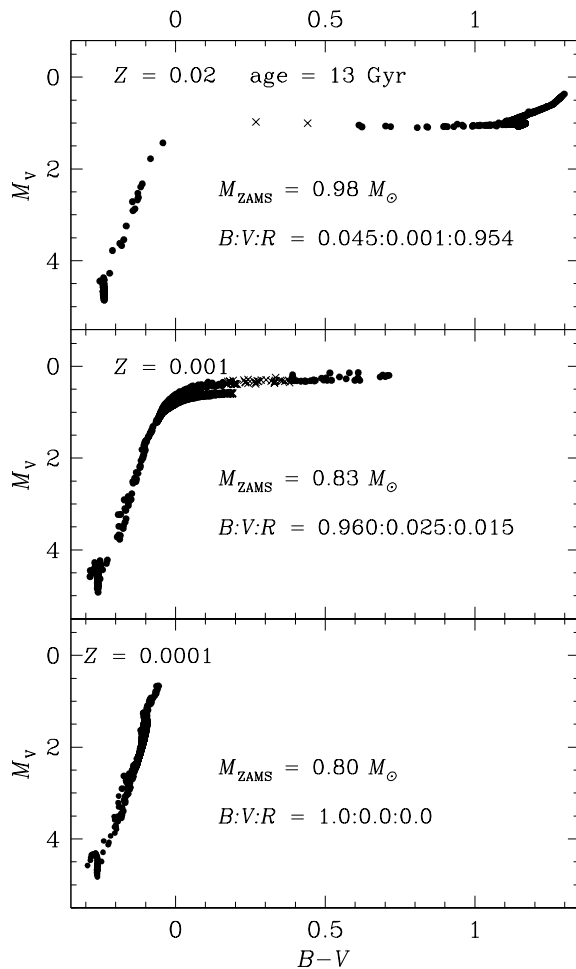


Fig. 1. Synthetic HB morphology produced by tidally enhanced stellar wind for different metallicities at a fixed age of 13 Gyr. The metallicities from the top panel to the bottom panel are $Z=0.02$, 0.001 , 0.0001 , for which the primary mass are 0.98 , 0.83 , and $0.80M_{\odot}$, respectively. HB stars in RR Lyrae strip (defined by the vertical region of $3.80 \leq \log T_{\text{eff}} \leq 3.875$ in the H-R diagram, Koopmann et al. 1994; Lee et al. 1990) are denoted by crosses. Other HB stars are denoted by solid dots. The label of $B : V : R$ in this figure is the number ratio of HB stars located in the region bluer than (or to the left of), within, and redder than (or to the right of) the RR Lyrae instability strip in the H-R diagram.

to settle on blue HB positions than for the metal-rich ones. Moreover, for the same envelope mass, the metal-poor HB stars have much higher effective temperatures on the ZAHB than the metal-rich ones owing their lower opacity in envelopes. This fact could also make the metal-poor HB stars occupy blue HB positions more easily than the metal-rich ones.

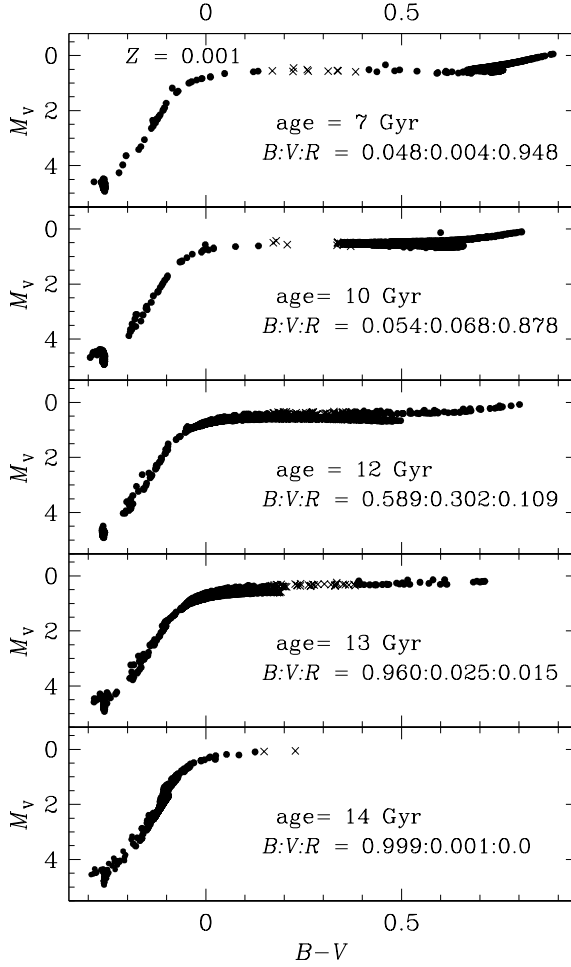


Fig. 2. Similar to Fig.1, but for different ages at $Z=0.001$. The M_{ZAMS} of the primary star from the top to bottom panels are 0.97, 0.89, 0.85, 0.83, and $0.80M_{\odot}$, which corresponds to cluster ages of 7, 10, 12, 13, and 14 Gyr, respectively.

3.3. Synthetic HB morphology in CMD for different ages

The synthetic HB morphology in CMD for different ages at a fixed metallicity of $Z = 0.001$ are obtained in a similar way to the one used in Section 3.2, but the value of M_{HF} and $M_{c,HB}$ for each sample star in this set of calculation are obtained by interpolating with the results in Table 3.

Figure.2 shows five synthetic HB in CMD with different ages of GCs at metallicity of $Z=0.001$. The M_{ZAMS} of the primary star in Fig.2 from the top to bottom panels are 0.97, 0.89, 0.85, 0.83, and $0.80M_{\odot}$. These five masses correspond to cluster ages of about 7, 10, 12, 13, and 14 Gyr, respectively. The label of $B : V : R$ in Fig.2 has the same meaning as in Fig.1.

One can see clearly in Fig.2 that, with the age increasing from the top to the bottom panel, more and more HB stars are located in blue and extreme HB. Especially in bottom panel of Fig.2, which corresponds to the largest cluster age of about 14 Gyr in our model calculations, the synthetic HB is nearly a whole blue HB, and no red HB stars are produced. Figure.2 indicates that old GCs will present bluer HB morphology than the young ones. This is because that old GCs have a lower stellar mass than the young ones at the RGB tip for a fixed metallicity. Therefore, the stars in old

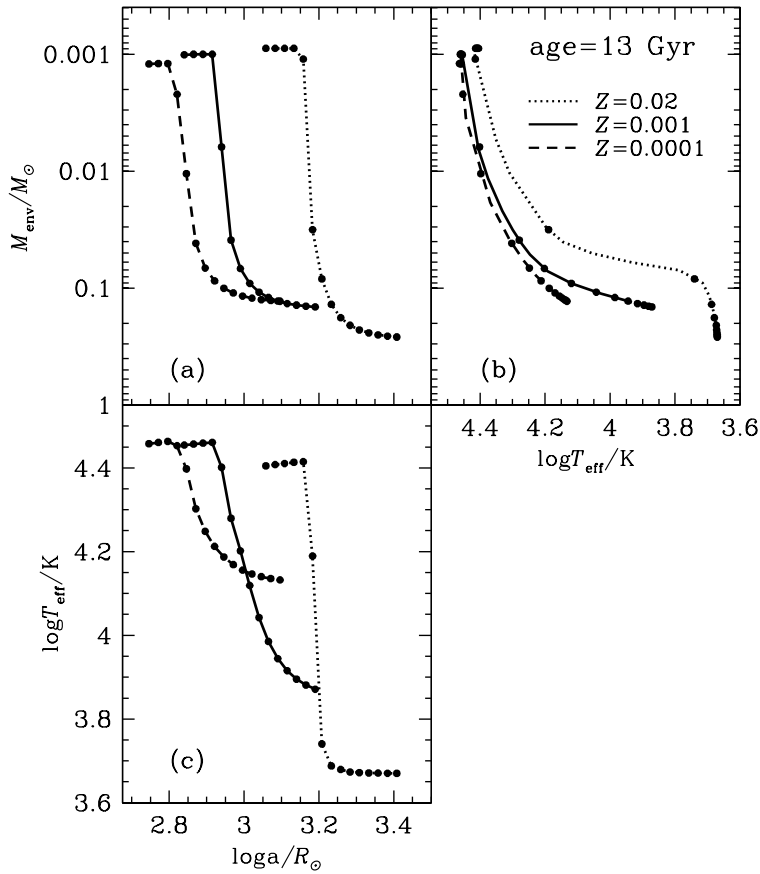


Fig. 3. Panel (a) gives the envelope mass distribution of ZAHB stars produced by the tidally enhanced stellar wind. Panel (b) shows the relationship between the envelope mass and effective temperature of ZAHB stars. Panel (c) presents the effective temperature distribution of ZAHB stars produced by the tidally enhanced stellar wind. The dashed, solid, and dotted curves in each panel correspond to the model calculations for three different metallicities as in Fig.1, namely $Z=0.0001$, 0.001 , 0.02 , respectively. The two adjacent solid dots in each curve of these three panels denote a fixed separation interval of $\Delta \log a/R_{\odot}=0.025$ (a is the separation of binary system).

GCs settle more easily on blue HB positions than the stars in young GCs if they follow the same mass-loss law on the RGB.

4. Discussion

4.1. Bimodality on HB

From the top panel of Fig.1, in which the metallicity is $Z=0.02$, one can see that there is a distinct gap between red and blue HB. However, this bimodal HB distribution is not seen clearly in our synthetic HB for $Z=0.001$ and 0.0001 in Fig.1, which indicates that metal-rich GCs are more likely to form a bimodal HB than the metal-poor ones. To discuss the physical reason for this result, we

present three panels in Fig.3. The dashed, solid and dotted curves in each panel correspond to the model calculations for three different metallicities as in Fig.1, namely $Z=0.0001$, 0.001 , and 0.02 .

Panel (a) gives the envelope mass distribution of ZAHB stars produced by the tidally enhanced stellar wind. Since the distribution of separation in $\log a$ is constant when the separation, a , is larger than $10 R_{\odot}$ (see Section 2.3), the number of the initial binary systems in each fixed separation interval (i.e., 0.025) is the same. Therefore, the higher the concentration of the solid dots in each curve, the more ZAHB stars will be produced in this envelope mass range. One can see clearly from panel (a) of Fig.3 that the envelope mass distributions produced by the tidally enhanced stellar wind for three different metallicities are similar and that the number of ZAHB stars with their envelope masses in the rough range of $0.003M_{\odot} \lesssim M_{\text{env}} \lesssim 0.06M_{\odot}$ is obviously less than the number of ZAHB stars with the envelope mass beyond this range.

Panel (b) of Fig.3 shows the relationship between the envelope mass and the effective temperatures of ZAHB stars. One can see clearly that, for $Z = 0.02$, a large gap is presented within the effective temperature range of $3.8 \lesssim \log T_{\text{eff}} \lesssim 4.3$. However, for $Z = 0.001$ and 0.0001 , the sparse area on ZAHB occupies a much narrower and bluer effective temperature range than that of $Z = 0.02$. This is because the opacity of metal-poor HB stars in their envelopes is less than the metal-rich ones. Furthermore, due to the decreasing sensitivity of $B - V$ color to effective temperature towards higher temperatures (Moehler 2010) and due to the vertical evolution of hot HB stars in H-R diagram (see Fig.1 in Paper I), the small gap on HB for metal-poor GCs in CMD may become obscure.

Panel (c) in Fig.3 is the combination of panels (a) and (b), which shows the relationship between the initial separations of binary systems and the effective temperatures of ZAHB stars produced by tidally enhanced stellar wind. One can see that the distribution of HB stars is clearly bimodal for $Z = 0.02$. However, this feature becomes more and more obscure with decreasing metallicity, which means that in our model calculation, metal-rich GCs are more likely to form a bimodal HB morphology than the metal-poor ones.

4.2. age-HBR diagram in GCs

One can see from Fig.2 that old GCs present bluer HB morphology than the young ones. To compare this result with the observation in GCs, we show in Fig.4 the relationship between the age of GCs in our Galaxy and the parameter, HBR , which is used to describe the HB morphology of GCs (Lee et al. 1990; Lee et al. 1994). The parameter, HBR , is defined as,

$$HBR = (B - R)/(B + V + R), \quad (3)$$

where B , V , and R have the same meanings as described in Section 3.2. The value of the parameter, HBR , is in the range of -1 to 1 . The value of -1 means that all HB stars settle on red HB; on the other hand, the value of 1 means that GC presents a whole blue HB. Therefore, the larger the HBR parameter, the bluer the HB morphology in GCs. The values of HBR parameter for GCs in Fig.4 are from the catalog of Harris (1996), and the age of GCs used in this figure is from Gratton et al. (2010)². To compare the observation with our results, we chose the GCs in the metallicity range of

² The relative ages of GCs in Gratton et al. (2010) are from Marin-Franch et al. (2009) and De Angeli et al. (2005).

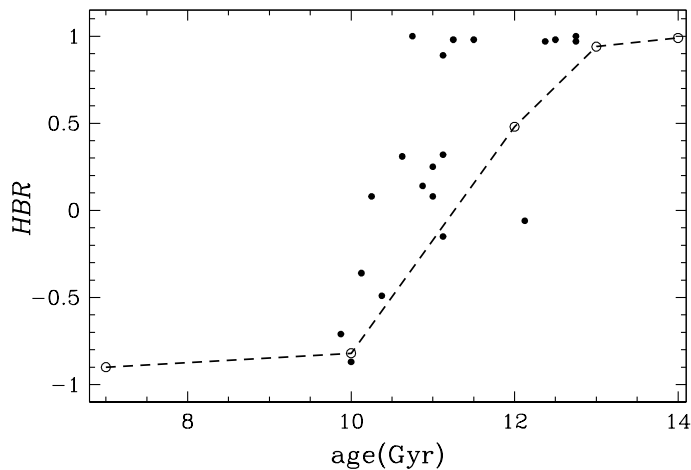


Fig. 4. The relationship between the age and the HB morphology parameter, HBR , in GCs. The solid circles are the selected GCs in our Galaxy, which are in the metallicity range of $-1.6 < [Fe/H] < -1.1$. The open circles denote our model calculations in Fig.2, which from left to right correspond to cluster ages of 7, 10, 12, 13, and 14 Gyr, respectively.

$-1.6 < [Fe/H] < -1.1$ in Fig.4, which is around the metallicity used in Fig.2 (i.e., $Z = 0.001$ or $[Fe/H] = -1.3$). This limit weakens the effect of metallicity on HB morphology, thus the effect of age on HB morphology could be revealed more clearly.

One can see in Fig.4 that, for the selected GCs in our Galaxy, the value of HBR increases with the increasing age of the GCs, which means the HB morphology becomes bluer when the ages of the GCs become older. This result is consistent with the one obtained from Fig.2, and also can be seen clearly from the dashed line in Fig.4. However, for a fixed age of GCs, our synthetic HB produced by a tidally enhanced stellar wind in Fig.4 is a little redder than the observed ones. This may be because we do not consider the common envelope (CE) and Roche lobe overflow (RLOF) processes in binary evolution for our calculations (see Section 3.1 and Paper I). These processes can produce EHB stars (Han et al. 2002, 2003), and thus make HB bluer.

We also adopted a different value of Reimers mass-loss efficiency (e.g., $\eta=0.25$, which is the value we used in Paper I) in our model calculations. We found that, for $\eta=0.25$, the result is similar to the one in Fig.4. However, to produce a blue HB morphology (e.g., $HBR \gtrsim 0.5$), the age of GCs should be greater than 15 Gyr. This indicates that $\eta=0.25$ is too small to produce the observed HB morphology in GCs. Renzini & Fusi Pecci (1988) demonstrated that observed HB morphologies in GCs with $Z \simeq 0.001$ demand $\eta = 0.4 \pm 0.04$. That is why we use the value of $\eta = 0.45$ in this paper, but it does not influence the results we obtained in Paper I, since we can obtain the same results using a little younger age of GCs for a higher value of η .

4.3. Effects of binary fraction on HB morphology

In our model calculations, all stars are in binary systems, but the binaries with long orbital periods are actually single stars. The separation distribution of binary systems described in Section 2.3 implies that about 50% of binary systems have orbital periods that all shorter than 100 yr. To inves-

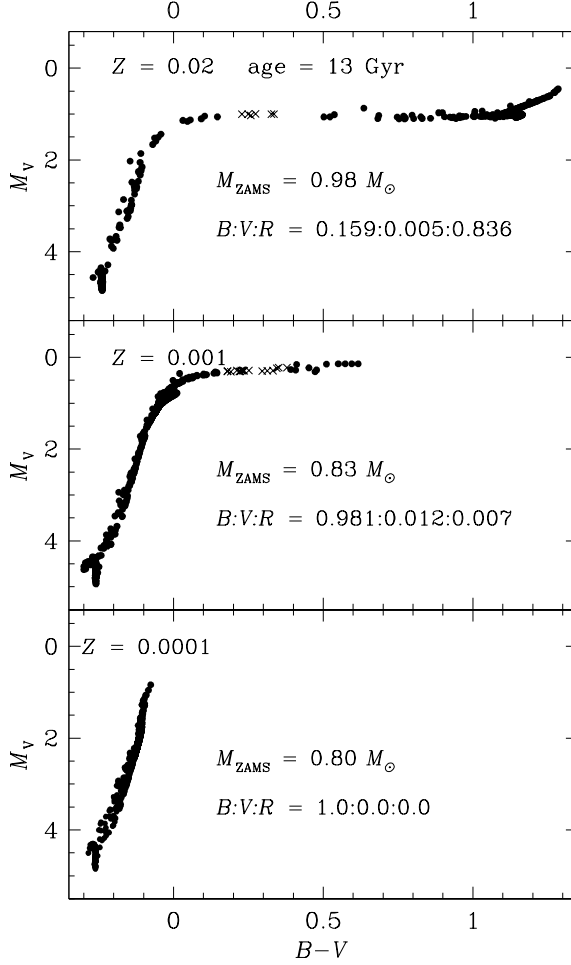


Fig. 5. Same as Fig.1, but with a higher binary fraction of 80% rather than 50%.

to investigate the effects of binary fractions on our final results, we also adopted various binary fractions in our calculations (i.e., 10%, 15%, 20%, 30%, and 80%)³. The result of model calculation for a binary fraction of 80% is shown in Figs.5 and 6. The input parameters in Figs.5 and 6 are the same as in Figs.1 and 2, except for the binary fraction.

By comparing Figs.5 and 1, one can see that, with the binary fraction increasing, the number ratio of HB stars bluer than the RR Lyrae instability strip increases, while the number ratio of red HB stars decreases. For example, in the top panel of Fig.5, the number ratio of HB stars bluer than RR Lyrae instability strip is 15.9%, as opposed to 4.5% in the top panel of Fig.1; while the number ratio of red HB stars is 83.6%, versus 95.4% in the top panel of Fig.1. We can also obtain this result by comparing Figs.6 and 2, and the model calculations for binary fraction of 10%, 15%, 20%, and 30% show similar results. These results indicate that higher binary fraction may make HB morphology become bluer. This is because the orbital period in which tidally enhanced stellar wind significantly affects mass loss of the primary star is from $\log P/\text{day} \approx 3.1$ to $\log P/\text{day} \approx 3.5$ (see Tables 2 and 3), and the orbital periods of binaries in this range are less than 100 yr. Therefore,

³ All these binary fractions are for the binary systems with their orbital periods less than 100 yr.

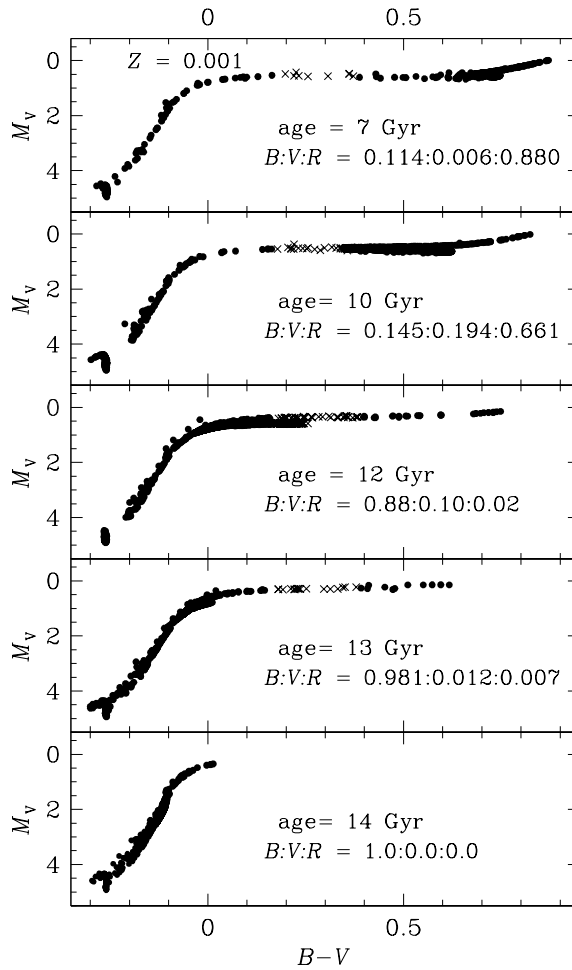


Fig. 6. Same as Fig.2, but with a higher binary fraction of 80% rather than 50%.

for a given total number of binary samples, when the fraction of binary systems with their binary orbital periods less than 100 yr increases, more primary stars will be influenced by tidally enhanced stellar winds, and then more blue and extreme HB stars will be produced.

Our results indicate that higher binary fraction may make the HB morphology become bluer, which implies that binary population is a possible second parameter candidate. However, Milone et al. (2012) estimate the binary fraction for 59 Galactic GCs by analyzing the number of stars located on the red side of the main-sequence fiducial line (also see Sollima et al. 2007). Moreover, they studied the relationship between the binary fraction and the HB morphology parameters, and conclude that there is weak or null impact of binary populations on HB morphology (see Fig.47 and Section 5.6.3 in their paper). At first glance, their results contradict ours. However, the sample GCs in Milone et al. (2012) have different metallicities and ages, which are very important parameters that affect HB morphology in GCs (Gratton et al. 2010; Dotter et al. 2010). Therefore, Milone et al. (2012) did not remove the effects of metallicity and age on HB morphology when studying the

effect of binary fraction on HB morphology, and this will significantly influence the final results⁴. On the other hand, our result that higher binary fraction may make HB morphology become bluer is obtained by comparing GCs with fixed metallicity and age but different binary fractions. This means that we removed the effects of metallicity and age when studying the effects of binary fraction on HB morphology. Thus, the results obtained by Milone et al. (2012) cannot exclude binary populations as a second parameter candidate that may affect HB morphology in GCs.

One can also see that, though the binary fraction is higher than in Fig.1, the synthetic HB for $Z=0.02$ in the top panel of Fig.5 still presents a distinct gap between red and blue HB, with very few of the HB stars located in RR Lyrae instability strip, (Similar results are obtained for other different binary fractions.) This result indicates that binary fraction may have little effect on the bimodality of HB, and the bimodality of HB may mainly depend on the metallicity of GCs (see our discussion in Section 4.1).

5. Conclusions

In this paper, we considered tidally enhanced stellar winds during binary evolution to study the effects on the HB morphology of GCs with different metallicities and ages. We found that metal-poor GCs should present bluer HB morphology than the metal-rich ones, and this is consistent with previous work. Furthermore, we found in our calculations that the envelope-mass distributions of ZAHB stars produced by a tidally enhanced stellar wind are very similar for different metallicities. However, the synthetic HB for $Z=0.02$ produced by tidally enhanced stellar wind presents a distinct gap between red and blue HB, while this feature is not seen clearly in the synthetic HB for $Z=0.001$ and 0.0001 . We also found that old GCs present bluer HB than the young ones, which is also consistent with previous work. We compared our results with the observation in the age-*HBR* diagram of GCs. Furthermore, we studied the effect of binary fraction on our final results, and found that higher binary fraction may make HB morphology become bluer. We finally discussed our results with recent observations.

Acknowledgements. We thank the anonymous referee for valuable comments and suggestions that helped us to improve the paper. This work is supported by the National Natural Science Foundation of China (Grant Nos.11033008, 11273053 and 11203065) and the Chinese Academy of Sciences (Grant No. KJXC2-YW-T24).

References

- Carretta, E., Bragaglia, A., Gratton, R. G.; et al. 2010, *A&A*, 516, A55
 Catelan, M. 2009, *Ap&SS*, 320, 261
 Chaboyer, B., Green, E. M., & Liebert, J. 1999, *AJ*, 117, 1360
 Chen, X. F., & Tout, C. A. 2007, *Chinese J. Astron. Astrophys.*, 7, 245
 Dalessandro, E., Salaris, M., Ferraro, F. R., et al. 2011, *MNRAS*, 410, 694
 D'Antona, F., & Caloi, V. 2004, *ApJ*, 611, 871
 De Angeli, F., Piotto, G., Cassisi, S. et al. 2005, *AJ*, 130, 116
 Dotter, A., Sarajedini, A., Anderson, J., et al. 2010, *ApJ*, 708, 698
 Dupree, A. K., Smith, G. H., Strader, J., et al. 2009, *AJ*, 138, 1485.

⁴ For example, we used a binary fraction of 10% in the calculation and found that, though the binary fraction is relatively low, the synthetic HB for $Z=0.0001$ at 13 Gyr is still a pure blue HB (e.g., $HBR=1$). It means that the effect of metallicity may mask the effect of binary fraction on HB morphology at very low metallicity.

- Eggleton, P. P. 1971, *MNRAS*, 151, 351
- Eggleton, P. P. 1972, *MNRAS*, 156, 361
- Eggleton, P. P. 1973, *MNRAS*, 163, 279
- Friel, E. D., & Janes, K. A. 1993, *A&A*, 267, 75
- Gratton, R. G., Carretta, E., & Bragaglia, A., 2012, *A&A Rev.*, 20, 50
- Gratton, R. G., Carretta, E., Bragaglia, A., et al. 2010, *A&A*, 517, A81
- Han, Z., Podsiadlowski, P., & Eggleton, P. P. 1994, *MNRAS*, 270, 121
- Han, Z., Podsiadlowski, Ph., Maxted, P. F. L., Marsh, T. R., & Ivanova, N. 2002, *MNRAS*, 336, 449
- Han, Z., Podsiadlowski, Ph., Maxted, P. F. L., & Marsh, T. R. 2003, *MNRAS*, 341, 669
- Harris, W. E. 1996, *AJ*, 112, 1487
- Kaluzny, J., & Rucinski, S. M. 1995, *A&AS*, 114, 1
- Kaluzny, J., & Udalski, A. 1992, *Acta Astron.*, 42, 29
- Koopmann, R. A., Lee, Y. W., Demarque, P., et al. 1994, *ApJ*, 423, 380
- Lee, H. C., Yoon, S. J., & Lee, Y. W. 2000, *AJ*, 120, 998
- Lee, Y. W., Demarque, P., & Zinn, R. 1990, *ApJ*, 350, 155
- Lee, Y. W., Demarque, P., & Zinn, R. 1994, *ApJ*, 423, 248
- Lei, Z., Chen, X., Zhang, F., & Han, Z. 2013, *A&A*, 549, A145, Paper I
- Lejeune, T., Cuisinier, F., & Buser R. 1997, *A&AS*, 125, 229
- Lejeune, T., Cuisinier, F., & Buser R. 1998, *A&AS*, 130, 65
- Liebert, J., Saffer, R. A., & Green, E. M. 1994, *AJ*, 107, 1408
- Marin-Franch, A., Aparicio, A., & Piotto, G., et al. 2009, *ApJ*, 694, 1498
- Milone, A. P., Piotto, G., Bedin, L. R., et al. 2012, *A&A*, 540, A16
- Moehler, S. 2010, *MmSAI*, 81,838
- Paxton, B., Bildsten, L., Dotter, A., et al. 2011, *ApJS*, 192, 3
- Percival, S. M., & Salaris, M. 2011, *MNRAS*, 412, 2445
- Peterson, R. C., & Green, E. M. 1998, *ApJ*, 502, L39
- Piotto, G., Bedin, L. R., Anderson, J., et al. 2007, *ApJ*, 661, L53
- Piotto, G.; Milone, A. P.; Anderson, J.; et al. 2012, *ApJ*, 760, 39
- Pols, O. R., Schröder, K. P., Hurley, J. P., et al. 1998, *MNRAS*, 298, 525
- Pols, O. R., Tout, C. A., Eggleton, P. P., & Han, Z. 1995, *MNRAS*, 274, 964
- Pols, O. R., Tout, C. A., Schröder, K. P., et al. 1997, *MNRAS*, 289, 869
- Reimers, D. 1975, *MSRSL*, 8, 369
- Renzini, A., & Fusi Pecci, F. 1988, *ARA&A*, 26, 245
- Rood, R. T. 1973, *ApJ*, 184, 815
- Sandage, A., & Wallerstein, G. 1960, *ApJ*, 131, 598
- Sollima, A., Beccari, G., Ferraro, F. R., et al. 2007, *MNRAS*, 380, 781
- Tout, C. A., & Eggleton, P. P. 1988, *MNRAS*, 231, 823
- Willson, L. A. 2000, *ARA&A*, 38, 573

Synthetic horizontal branch morphology for different metallicities and ages under tidally enhanced stellar wind

Z. Lei^{1,2,3}, F. Zhang^{1,2}, H. Ge^{1,2}, and Z. Han^{1,2}

¹ National Astronomical Observatories/Yunnan Observatory, the Chinese Academy of Sciences, KunMing 650011, China

e-mail: lzx2008@ynao.ac.cn

² Key Laboratory for the Structure and Evolution of Celestial Objects, the Chinese Academy of Sciences, Kunming 650011, China

³ University of the Chinese Academy of Sciences, Beijing 100049, China

Received ; accepted

ABSTRACT

Context. It is believed that some other parameters, except for metallicity (the first parameter), are needed to explain the horizontal branch (HB) morphology of globular clusters (GCs). Furthermore, these parameters are considered to be correlated with the mass loss of the red giant branch (RGB) stars. Unfortunately, the physics of mass loss on the RGB is poorly understood at present. In our previous work, we proposed that tidally enhanced stellar wind during binary evolution may affect the HB morphology by enhancing the mass loss of the red giant primary and that we can reproduce the basic morphology of HB in GCs.

Aims. We did not consider the effects of other important parameters (e.g., metallicity, age, etc) in our final results there. As a further study, we now investigate the effects of metallicity and age on HB morphology by considering tidally enhanced stellar winds during binary evolution.

Methods. We incorporated the tidally enhanced-stellar-wind model of Tout & Eggleton into Eggleton's stellar evolution code to study the binary evolution. A group of binary system samples were generated by Monte Carlo simulations. The position of each sample star in a color-magnitude diagram was obtained by transforming temperature and luminosity into $B - V$ color and absolute magnitude. To study the effects of metallicity and age on our final results, we conducted two sets of model calculations: (i) for a fixed age, we used three metallicities, namely $Z=0.0001$, 0.001 and 0.02 . (ii) for a fixed metallicity, $Z = 0.001$, we used five ages in our model calculations: 14, 13, 12, 10, 7 Gyr.

Results. We found that HB morphology of GCs becomes bluer with decreasing **metallicity**, and old GCs present bluer HB morphology than young ones. These results are consistent with previous work. Although the envelope-mass distributions of zero-age HB stars produced by tidally enhanced stellar wind are similar for different metallicities, the synthetic HB under tidally enhanced stellar wind for $Z=0.02$ presented a distinct gap between red and blue HB. However, this feature was not seen clearly in the synthetic HB for $Z=0.001$ and 0.0001 . **We also found that binary fractions may make HB morphology become bluer, and we discuss the results with recent observations.**

Key words. Clusters: globular clusters - star: horizontal branch - star: stellar evolution

1. Introduction

The color distribution of horizontal branch (HB) stars in the color-magnitude diagram (CMD) of globular clusters (GCs), which is defined as HB morphology, is a long-standing problem in stellar evolution. Although the most important factor affecting HB morphology is identified as the metallicity (called the first parameter, Sandage & Wallerstein 1960), other parameters are also believed to play an important role in this problem. These parameters are called the second parameter (2P). However, the nature of the 2P is still unknown. Many 2P candidates have been proposed in the past five decades, such as: cluster age (Lee et al., 1994), internal rotation and helium mixing (Sweigart, 1997), helium self-enrichment (D'Antona et al., 2002; D'Antona et al., 2005; D'Antona & Caloi, 2004, 2008), core density or concentration (Fusi Pecci et al., 1993; Buonanno et al., 1997), presence of a planetary system (Soker, 1998; Soker et al. 2000, 2001, 2007); cluster mass (Recio-Blanco et al. 2006), etc. **Recently, some researchers suggested that, except for metallicity, age may be the main global parameter affecting HB morphology in GCs, while some other parameters are needed to be as the third parameter, such as helium abundance, central density, etc (Gratton et al. 2010; Dotter et al. 2010). Moreover, the second parameter problem is considered to be correlated with multiple populations discovered in GCs (Piotto et al. 2007, 2012; Carretta et al. 2010; Gratton, Carretta & Bragaglia, 2012).**

Mass loss on the red giant branch (RGB) is a very important process to understand the 2P problem in GCs (Catelan 2009), since the color distribution of HB stars in CMD depends on their envelope masses, while the envelope mass is determined by the mass loss on the RGB. Unfortunately, the physics of mass loss on the RGB is poorly known at present (Willson 2000; Dupree et al. 2009). Therefore, in order to reproduce different parts of the HB in GCs, most of the 2P candidates based on single-star evolution need to assume a mass-loss dispersion on the RGB (e.g., Gaussian distribution of mass with a mass dispersion for HB stars; Lee, Yoon & Lee 2000; Lee et al. 1994; D'Antona & Caloi, 2004; Percival & Salaris 2011). The assumption of mass-loss dispersion, however, is arbitrary and without any physical justification.

In our previous work (Lei et al. 2013; hereafter Paper I), we proposed that tidally enhanced stellar wind during binary evolution may affect the HB morphology in GCs by enhancing the mass loss of the red giant primary. In a red giant binary system, the stellar wind of the red giant primary may be tidally enhanced by the secondary. The exact mass loss of the primary stars on the RGB depends on the initial binary orbital period. Therefore different initial binary orbital periods lead to different mass loss of the primary on the RGB. After the ignition of helium in their cores, the primary stars locate on different positions of the HB. In Paper I, under the consideration of tidally enhanced stellar wind, and without any additional assumptions of mass-loss dispersion on the RGB, we can reproduce the basic HB morphology of GCs, in which red, blue and extreme HB are all populated. However, we do not know exactly how other important parameters (e.g., metallicity and age) affect our results obtained in Paper I. As a further study of our previous work, in this paper, using the same method described in Paper I, we study the effects on HB morphology for different metallicities and ages, under the consideration of tidally enhanced stellar wind during binary evolution.

The structure of this paper is as follows. In Section 2, we introduce the method and code used in this paper. Our results are given in Section 3. A discussion and conclusions are given in Section 4 and Section 5, respectively.

2. Method and code

As described in Paper I, in this work, we also incorporate tidally enhanced stellar wind during binary evolution (see Sect 2.2) into Eggleton’s stellar evolution code (see Sect 2.1) to calculate the stellar mass and the helium core mass of the primary star at the helium flash (hereafter M_{HF} and $M_{\text{c,HF}}$, respectively). Then, M_{HF} , $M_{\text{c,HF}}$, and a lifetime spent on the HB are used to obtain the exact position of the primary star (e.g., effective temperature and luminosity) on the HB in the Hertzsprung-Russell (H-R) diagram by interpolating among constructed HB evolutionary tracks. All the HB evolutionary tracks are constructed using modules for experiments in stellar astrophysics (MESA; Paxton et al. 2011; see Paper I for **details**). Finally, we transform the effective temperature and luminosity of each HB star into $B - V$ colors and absolute magnitudes, M_V , to obtain the synthetic HB morphology in CMD. All these processes are carried out for different metallicities and ages to investigate the effects of these two parameters on the final results.

2.1. Stellar evolution code

Eggleton’s stellar evolution code **was** developed in the early 1970s (Eggleton 1971, 1972, 1973). This code has been updated with the latest input physics over the past four decades (Han et al. 1994; Pols et al. 1995, 1998). Now, this code is being applied extensively in the field of stellar evolution. In our calculations, the ratio of mixing length to local pressure scale height, $\alpha = l/H_P$, is set to 2.0. The convective overshooting parameter, δ_{ov} , is set to 0.12 (Pols et al. 1997). The opacity used in our calculations was compiled by Chen & Tout (2007). We obtain the initial hydrogen mass fraction, X , by $X = 0.76 - 3Z$, where Z is the metallicity (Pols et al. 1998).

2.2. Tidally enhanced stellar wind

We use the same equation as in Paper I to describe the tidally enhanced stellar wind during binary evolution,

$$\dot{M} = -\eta 4 \times 10^{-13} (RL/M) \{1 + B_w \times \min[(R/R_L)^6, 1/2^6]\}, \quad (1)$$

where η is the Reimers mass-loss efficiency, R_L is the radius of the Roche lobe, B_w is the tidal enhancement efficiency, and R , L , M are in solar units. This form of stellar wind was first suggested by Tout & Eggleton (1988) to explain the mass inversion phenomenon found in some RS CVn binary systems (see Paper I for detail). We incorporate equation (1) into Eggleton’s stellar evolution code to calculate M_{HF} and $M_{\text{c,HF}}$ of the primary star.

From our previous result in Paper I, the HB morphology is not very sensitive to the tidal enhancement parameter, B_w . For this reason, B_w is set to 10000 (e.g., the typical value used in Tout & Eggleton 1988) in all sets of calculations in this paper. Reimers mass-loss efficiency (Reimers 1975), η , is set to 0.45 (see the discussion in Section 4.2). To study the effects of metallicity and age on the HB morphology by considering tidally enhanced stellar wind, we carry out two sets of calculations: (i) for a fixed age of 13 Gyr, we use three different metallicities, namely $Z=0.0001$,

Table 1. Information for the two sets of calculations in this paper.

	Z	$M_{\text{ZAMS}}(M_{\odot})$	age (Gyr)
set(i)	0.0001	0.80	13
	0.001	0.83	13
	0.02	0.98	13
set(ii)	0.001	0.80	14
	0.001	0.83	13
	0.001	0.85	12
	0.001	0.89	10
	0.001	0.97	7

0.001, and 0.02. For these three metallicities, the stellar mass of the primary at zero-age main sequence (hereafter M_{ZAMS}) are 0.80, 0.83 and $0.98M_{\odot}$ respectively. (ii) For a fixed metallicity of GCs, $Z=0.001$, we use five M_{ZAMS} in our model calculations, namely 0.80, 0.83, 0.85, 0.89, and $0.97M_{\odot}$. These five masses correspond to cluster ages of 14, 13, 12, 10, and 7 Gyr, respectively. The **detailed** information for the two sets of calculations are shown in Table 1. The columns from left to right provide the metallicity, M_{ZAMS} , and the age of the primary star at helium flash, respectively. The results of the two sets of calculations are given in Tables 2 and 3 (see Section 3.1).

The mass ratio of primary to secondary is set to 1.6 (We used different mass ratios of primary to secondary in Paper I, but it has little influence on our results.) We assume that the mass accreted by the secondary from the stellar wind is retained in the binary system, and the angular momentum that **leaves** the binary system due to the stellar wind **is** attributed to the primary star.

2.3. Initial binary samples

To obtain the synthetic HB morphology in CMD, we generate several groups of binary systems, in which the metallicity and M_{ZAMS} of the primary stars correspond to the values given in Table 1. The mass ratio of primary to secondary is set to 1.6 (see Section 2.2). The initial orbital periods of all binary systems are produced by Monte Carlo simulations. The distribution of separation in binary is constant in $\log a$ (a is the separation) and falls off smoothly at small separations,

$$a \cdot n(a) = \begin{cases} \alpha_{\text{sep}}(a/a_0)^m, & a \leq a_0, \\ \alpha_{\text{sep}}, & a_0 < a < a_1, \end{cases} \quad (2)$$

where $\alpha_{\text{sep}} \approx 0.07$, $a_0 = 10 R_{\odot}$, $a_1 = 5.75 \times 10^6 R_{\odot} = 0.13 \text{ pc}$ and $m \approx 1.2$. This distribution implies that the number of wide binaries per logarithmic interval are equal and that about 50% of stellar systems have orbital periods less than 100 yr (Han et al. 2003).

3. Results

3.1. M_{HF} and $M_{\text{c, HF}}$ of the primary star for different metallicities and ages.

Table 2 shows the results of our model calculation for different metallicities, and it gives the M_{HF} , $M_{\text{c, HF}}$, and the envelope mass of the primary stars at the helium flash (M_{env}) with various initial binary orbital periods at a fixed age of 13 Gyr. The results in Table 2 correspond to the calculation

of set (i) (see Section 2.2). Recall that B_w is set to 10^4 and η is set to 0.45. The mass ratio of primary-to-secondary, q , is set to be 1.6. The columns from left to right provide the initial orbital periods, M_{HF} , $M_{\text{c,HF}}$, and M_{env} , respectively.

For each metallicity, the first binary orbital period in Table 2 is a minimum period (e.g., $\log P/\text{day} = 3.126$ for $M_{\text{ZAMS}} = 0.8M_{\odot}$ at metallicity of $Z = 0.0001$), above which a helium flash could take place. For orbital periods shorter than this critical value¹, the primary stars experience too much mass loss on the RGB due to the tidally enhanced stellar wind, and fail to ignite helium in their cores. Therefore, these primary stars will not undergo the HB phase and evolve into helium white dwarf (WD) cooling curve directly. With the increase in binary orbital period, the amount of mass loss of the primary star on the RGB decreases for each metallicity. When the initial binary orbital period is long enough, the tidally enhanced stellar wind becomes unimportant and has little effect on the mass loss of red giant primary (One can see that the M_{env} of primary stars with $\log P/\text{day} = 3.55$ and $\log P/\text{day}=10.0$ for $M_{\text{ZAMS}} = 0.8M_{\odot}$ at the metallicity of $Z = 0.0001$ are nearly the same, which means that they experience nearly the same amount of mass loss on the RGB.) At this time, the primary star just loses its envelope mass through Reimers mass-loss law (Reimers 1975).

Similar to Table 2, Table 3 presents our model calculation results for different ages at metallicity of $Z=0.001$, which corresponds to the calculation of set (ii) (see Section 2.2).

3.2. Synthetic HB morphology in CMD for different metallicities

To obtain the position of each sample star on the HB in the H-R diagram (e.g., effective temperatures and luminosities), we need to know M_{HF} , $M_{\text{c,HF}}$, and the time spent on HB phase **which means how long the HB star has been evolved from zero-age HB (ZAHB)**. The value of M_{HF} and $M_{\text{c,HF}}$ for each primary star in this set of calculation are obtained by interpolating with the results presented in Table 2. The time spent on the HB is generated by a uniform random number between 0 and the HB lifetime, τ_{HB} (Rood 1973; Lee et al. 1990; Dalessandro et al. 2011). Here, τ_{HB} is set to be the lifetime of HB star with the lowest stellar mass among the constructed HB evolutionary tracks, which means that this star **has** the longest lifetime on the HB. Therefore, some of HB stars are given a time longer than their lifetimes on the HB, and these stars are considered to evolve into the next evolutionary phase (e.g., AGB or WD). This process is equivalent to the scenario that stars enter the HB from the RGB at a constant rate (see Lee et al. 1990). We use M_{HF} , $M_{\text{c,HF}}$, and the time spent on HB phase to obtain the exact position of each primary star on HB in the H-R diagram by interpolating among constructed HB evolutionary tracks. After that, we transform the temperature and luminosity of each HB star into $B - V$ color and absolute magnitude, M_V , using the Basel stellar spectra library (Lejeune et al. 1997, 1998). Finally, we obtain the synthetic HB in CMD.

Figure.1 shows the synthetic HB for three different metallicities under the tidally enhanced stellar wind. The metallicities from the top to bottom panels in Fig.1 are $Z=0.02$, 0.001, and 0.0001, respectively. The corresponding M_{ZAMS} are 0.98, 0.83, and $0.80M_{\odot}$. In the top panel of Fig.1, the

¹ If the binary orbital period is short enough to make the the primary star fill its Roche lobe, then a Roche lobe overflow (RLOF) or a common envelope (CE) will begin in this binary system, but this is beyond the scope of present work.

Table 2. M_{HF} , $M_{\text{c,HF}}$, and M_{env} of the primary with various initial binary orbital periods for different metallicities at a fixed age of 13 Gyr. Here, $B_w = 10000$, $\eta = 0.45$, $q = 1.6$.

$\log P/\text{day}$	$M_{\text{HF}}(M_{\odot})$	$M_{\text{c,HF}}(M_{\odot})$	$M_{\text{env}}(M_{\odot})$
<hr/>			
$Z=0.0001, M_{\text{ZAMS}} = 0.80 M_{\odot}, \text{age}=13 \text{ Gyr}$			
3.1260	0.4869	0.4854	0.0015
3.1500	0.4904	0.4890	0.0014
3.2000	0.4976	0.4964	0.0012
3.2500	0.5047	0.5018	0.0029
3.3000	0.5328	0.5024	0.0304
3.3500	0.5688	0.5022	0.0666
3.4000	0.5932	0.5021	0.0911
3.4500	0.6088	0.5020	0.1068
3.5000	0.6186	0.5019	0.1167
3.5500	0.6247	0.5018	0.1229
10.000	0.6351	0.5017	0.1334
<hr/>			
$Z=0.001, M_{\text{ZAMS}} = 0.83 M_{\odot}, \text{age}=13 \text{ Gyr}$			
3.2590	0.4725	0.4714	0.0011
3.3000	0.4783	0.4774	0.0009
3.3500	0.4854	0.4845	0.0009
3.4000	0.4926	0.4895	0.0031
3.4500	0.5309	0.4893	0.0416
3.5000	0.5677	0.4892	0.0785
3.5500	0.5935	0.4891	0.1044
3.6000	0.6103	0.4890	0.1213
3.6500	0.6208	0.4889	0.1319
10.000	0.6386	0.4887	0.1499
<hr/>			
$Z=0.02, M_{\text{ZAMS}} = 0.98 M_{\odot}, \text{age}=13 \text{ Gyr}$			
3.5500	0.4504	0.4496	0.0008
3.6000	0.4571	0.4563	0.0008
3.7000	0.4709	0.4699	0.0010
3.7500	0.5171	0.4703	0.0468
3.8000	0.5910	0.4703	0.1207
3.8500	0.6491	0.4702	0.1789
3.9000	0.6853	0.4701	0.2152
3.9500	0.7072	0.4700	0.2372
4.0000	0.7206	0.4699	0.2507
4.5000	0.7421	0.4698	0.2723
10.000	0.7423	0.4698	0.2725
<hr/>			

synthetic HB has a high metallicity of $Z=0.02$. Most of HB stars in this panel locate in red HB (e.g., 95%), while stars in blue and extreme HB are just about 5%. One can see clearly in this panel that there is a distinct gap between red and blue HB, and a few of HB stars **are located** in the RR Lyrae instability strip. However, this bimodal HB morphology is not presented clearly in the other two panels of Fig.1. We discuss this result in Section 4.1. For the whole figure, with the metallicity decreasing from the top to bottom panels, more and more HB stars settle on blue and extreme HB. For the extreme case, in the bottom panel of Fig.1, which has the lowest metallicity of $Z=0.0001$ in our calculations, all HB stars **are located** in the region that is bluer than the RR Lyrae instability strip, with no red HB stars and RR Lyrae stars are produced. Figure.1 shows the typical effect of metallicity (the first parameter) on HB morphology in GCs, which is that metal-poor GCs

Table 3. M_{HF} , $M_{\text{c,HF}}$ and M_{env} of the primary with various initial binary orbital periods for different ages at $Z = 0.001$. Here, $B_w = 10000$, $\eta = 0.45$, $q = 1.6$.

$\log P/\text{day}$	$M_{\text{HF}}(M_{\odot})$	$M_{\text{c,HF}}(M_{\odot})$	$M_{\text{env}}(M_{\odot})$
<hr/>			
Z=0.001,	$M_{\text{ZAMS}} = 0.80 M_{\odot}$,	age=14 Gyr	
3.2980	0.4734	0.4724	0.0010
3.3600	0.4817	0.4808	0.0009
3.4200	0.4894	0.4884	0.0010
3.4500	0.4933	0.4902	0.0031
3.5000	0.5210	0.4900	0.0310
3.5500	0.5463	0.4899	0.0564
3.6000	0.5641	0.4898	0.0743
3.6500	0.5758	0.4897	0.0861
10.000	0.5959	0.4896	0.1063
<hr/>			
Z=0.001,	$M_{\text{ZAMS}} = 0.83 M_{\odot}$,	age=13 Gyr	
3.2590	0.4725	0.4714	0.0011
3.3000	0.4783	0.4774	0.0009
3.3500	0.4854	0.4845	0.0009
3.4000	0.4926	0.4895	0.0031
3.4500	0.5309	0.4893	0.0416
3.5000	0.5677	0.4892	0.0785
3.5500	0.5935	0.4891	0.1044
3.6000	0.6103	0.4890	0.1213
3.6500	0.6208	0.4889	0.1319
10.000	0.6386	0.4887	0.1499
<hr/>			
Z=0.001,	$M_{\text{ZAMS}} = 0.85 M_{\odot}$,	age=12 Gyr	
3.2360	0.4719	0.4708	0.0011
3.3000	0.4813	0.4803	0.0010
3.3500	0.4886	0.4875	0.0011
3.4000	0.5146	0.4889	0.0257
3.4500	0.5637	0.4889	0.0748
3.5000	0.6008	0.4887	0.1121
3.5500	0.6251	0.4886	0.1365
3.6000	0.6405	0.4884	0.1521
3.6500	0.6502	0.4883	0.1619
10.000	0.6662	0.4883	0.1779
<hr/>			
Z=0.001,	$M_{\text{ZAMS}} = 0.89 M_{\odot}$,	age =10 Gyr	
3.1950	0.4708	0.4698	0.0010
3.2500	0.4792	0.4793	0.0009
3.3000	0.4869	0.4859	0.0010
3.3500	0.5162	0.4879	0.0283
3.4000	0.5832	0.4879	0.0953
3.4500	0.6338	0.4877	0.1461
3.5000	0.6665	0.4876	0.1789
3.5500	0.6868	0.4875	0.1993
3.6000	0.6993	0.4874	0.2119
3.6500	0.7071	0.4874	0.2197
10.000	0.7201	0.4873	0.2328
<hr/>			
Z=0.001,	$M_{\text{ZAMS}} = 0.97 M_{\odot}$,	age =7 Gyr	
3.1250	0.4687	0.4677	0.0010
3.2000	0.4808	0.4799	0.0009
3.2500	0.4894	0.4861	0.0033
3.3000	0.5827	0.4862	0.0965
3.3500	0.6741	0.4861	0.1880
3.4000	0.7319	0.4860	0.2459
3.4500	0.7669	0.4859	0.2810
3.5000	0.7882	0.4858	0.3024
3.5500	0.8013	0.4858	0.3155
3.6000	0.8094	0.4857	0.3237
10.000	0.8227	0.4856	0.3371

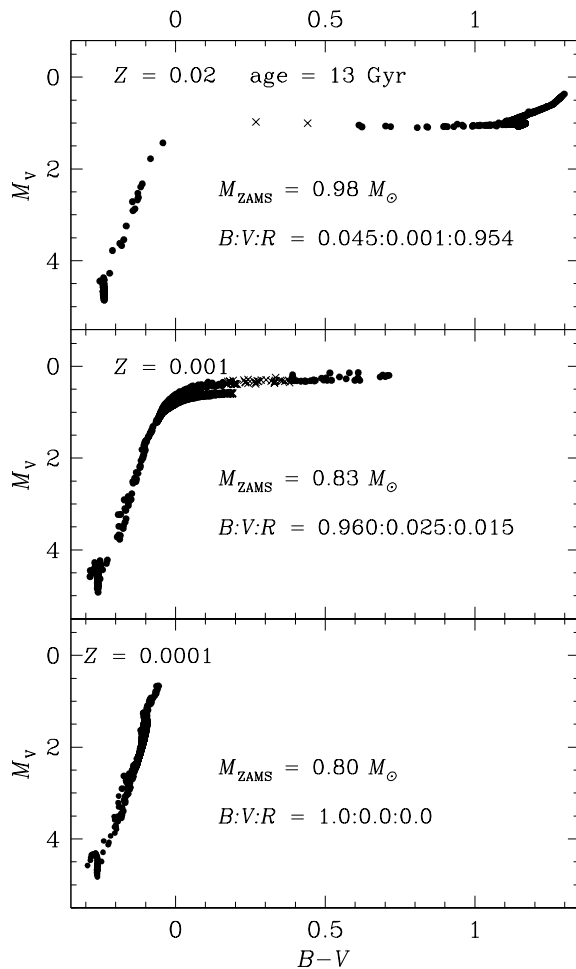


Fig. 1. Synthetic HB morphology produced by tidally enhanced stellar wind for different metallicities at a fixed age of 13 Gyr. The metallicities from the top panel to the bottom panel are $Z=0.02$, 0.001 , 0.0001 , for which the primary mass are 0.98 , 0.83 , and $0.80M_{\odot}$, respectively. HB stars in RR Lyrae strip (defined by the vertical region of $3.80 \leq \log T_{\text{eff}} \leq 3.875$ in the H-R diagram, Koopmann et al. 1994; Lee et al. 1990) are denoted by crosses. Other HB stars are denoted by solid dots. The label of $B : V : R$ in this figure is the number ratio of HB stars located in the region bluer than (or to the left of), within, and redder than (or to the right of) the RR Lyrae instability strip in the H-R diagram.

present bluer HB morphology than the metal-poor ones. This is because the metal-poor GCs have a lower stellar mass than the metal-rich ones at the tip of RGB for a fixed cluster age. As a result, assuming that the mass-loss law on the RGB is the same, it is much easier for the metal-poor stars to settle on blue HB positions than for the metal-rich ones. Moreover, for the same envelope mass, the metal-poor HB stars have much higher effective temperatures on the ZAHB than the metal-rich

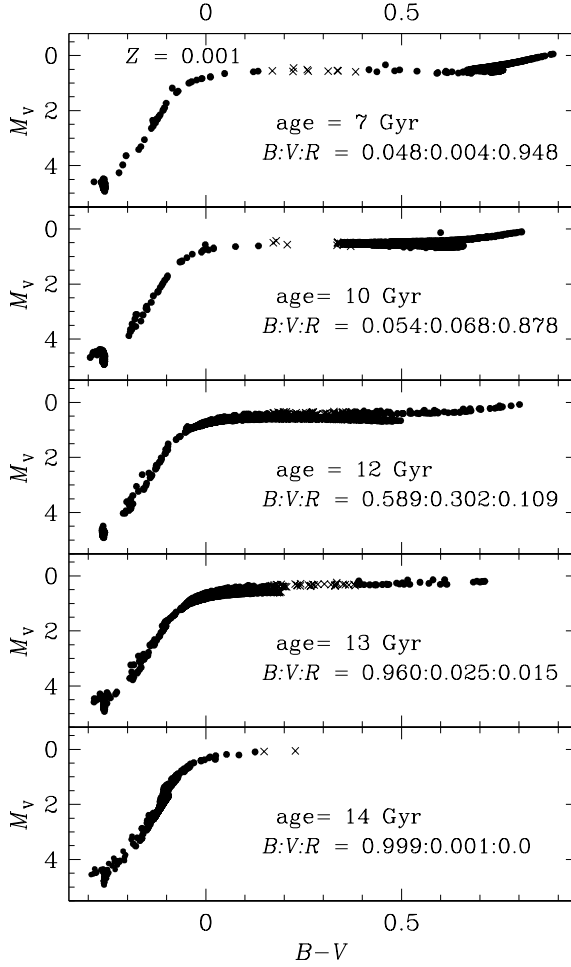


Fig. 2. Similar to Fig.1, but for different ages at $Z=0.001$. The M_{ZAMS} of the primary star from the top to bottom panels are $0.97, 0.89, 0.85, 0.83,$ and $0.80M_{\odot}$, which corresponds to cluster ages of 7, 10, 12, 13, and 14 Gyr, respectively.

ones owing their lower opacity in envelopes. This fact could also make the metal-poor HB stars occupy blue HB positions more easily than the metal-rich ones.

3.3. Synthetic HB morphology in CMD for different ages

The synthetic HB morphology in CMD for different ages at a fixed metallicity of $Z = 0.001$ are obtained in a similar way to the one used in Section 3.2, but the value of M_{HF} and $M_{\text{c,HF}}$ for each sample star in this set of calculation are obtained by interpolating with the results in Table 3.

Figure.2 shows five synthetic HB in CMD with different ages of GCs at metallicity of $Z=0.001$. The M_{ZAMS} of the primary star in Fig.2 from the top to bottom panels are $0.97, 0.89, 0.85, 0.83,$ and $0.80M_{\odot}$. These five masses correspond to cluster ages of about 7, 10, 12, 13, and 14 Gyr, respectively. The label of $B : V : R$ in Fig.2 has the same meaning as in Fig.1.

One can see clearly in Fig.2 that, with the age increasing from the top to the bottom panel, more and more HB stars **are located** in blue and extreme HB. Especially in bottom panel of Fig.2, which corresponds to the largest cluster age of about 14 Gyr in our model calculations, the synthetic HB

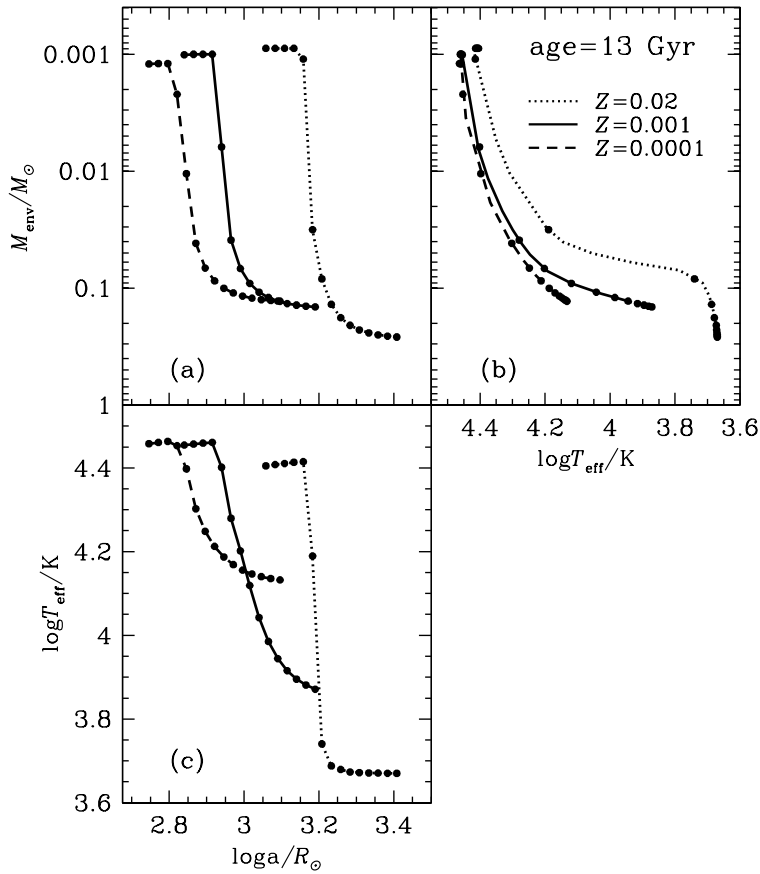


Fig. 3. Panel (a) gives the envelope mass distribution of ZAHB stars produced by the tidally enhanced stellar wind. Panel (b) shows the relationship between envelope mass and effective temperature of ZAHB stars. Panel (c) presents the effective temperature distribution of ZAHB stars produced by the tidally enhanced stellar wind. The dashed, solid and dotted curves in each panel correspond to the model calculations for three different metallicities as in Fig.1, namely $Z=0.0001, 0.001, 0.02$, respectively. The two adjacent solid dots in each curve of these three panels denote a fixed separation interval of $\Delta \log a/R_{\odot}=0.025$ (a is the separation of binary system).

is nearly a whole blue HB, and no red HB stars are produced. Figure.2 indicates that old GCs will present bluer HB morphology than the young ones. This is because that old GCs have a lower stellar mass than the young ones at the RGB tip for a fixed metallicity. Therefore, the stars in old GCs settle more easily on blue HB positions than the stars in young GCs if they follow the same mass-loss law on the RGB.

4. Discussion

4.1. Bimodality on HB

From the top panel of Fig.1, in which the metallicity is $Z=0.02$, one can see that there is a distinct gap between red and blue HB. However, this bimodal HB distribution is not seen clearly in our synthetic HB for $Z=0.001$ and 0.0001 in Fig.1, which indicates that metal-rich GCs are more likely to form a bimodal HB than the metal-poor ones. To discuss the physical reason for this result, we present three panels in Fig.3, namely panel (a), panel (b) and panel (c), respectively. The dashed, solid and dotted curves in each panel correspond to the model calculations for three different metallicities as in Fig.1, namely $Z=0.0001$, 0.001 and 0.02 , respectively. The two adjacent solid dots in each curve of these three panels denote a fixed separation interval of $\Delta \log a/R_{\odot}=0.025$ (a is the separation of binary systems).

Panel (a) gives the envelope mass distribution of ZAHB stars produced by the tidally enhanced stellar wind. Since the distribution of separation in $\log a$ is constant when the separation, a , is larger than $10 R_{\odot}$ (see Section 2.3), the number of the initial binary systems in each fixed separation interval (i.e., 0.025) is the same. Therefore, **the bigger the** concentration of the solid dots in each curve, **the more** ZAHB stars will be produced in this envelope mass range. One can see clearly from panel (a) of Fig.3 that the envelope mass distributions produced by the tidally enhanced stellar wind for three different metallicities are similar, that the number of ZAHB stars with their envelope masses in the rough range of $0.003M_{\odot} \lesssim M_{\text{env}} \lesssim 0.06M_{\odot}$ is obviously less than the number of ZAHB stars with the envelope mass beyond this range.

Panel (b) of Fig.3 shows the relationship between the envelope mass and the effective temperatures of ZAHB stars. One can see clearly that, for $Z = 0.02$, a large gap is presented within the effective temperature range of $3.8 \lesssim \log T_{\text{eff}} \lesssim 4.3$. However, for $Z = 0.001$ and 0.0001 , the sparse area on ZAHB occupies a much narrower and bluer effective temperature range than that of $Z = 0.02$ (This is because the opacity of metal-poor HB stars in their envelopes is smaller than the metal-rich ones). Furthermore, due to the decreasing sensitivity of $B - V$ color to effective temperature towards higher temperatures (Moehler 2010), and due to the vertical evolution of hot HB stars in H-R diagram (see Fig.1 in Paper I), the small gap on HB for metal-poor GCs in CMD may become obscure.

Panel (c) in Fig.3 is the combination of panel (a) and panel (b), which shows the relationship between the initial separations of binary systems and the effective temperatures of ZAHB stars produced by tidally enhanced stellar wind. One can see that the distributions of HB stars is clearly bimodal for $Z = 0.02$. However, this feature becomes more and more obscure with decreasing metallicity, which means that in our model calculation, meta-rich GCs are more likely to form a bimodal HB morphology than the metal-poor ones.

4.2. age-HBR diagram in GCs

One can see from Fig.2 that old GCs present bluer HB morphology than the young ones. To compare this result with the observation in GCs, we show in Fig.4 the relationship between the age of

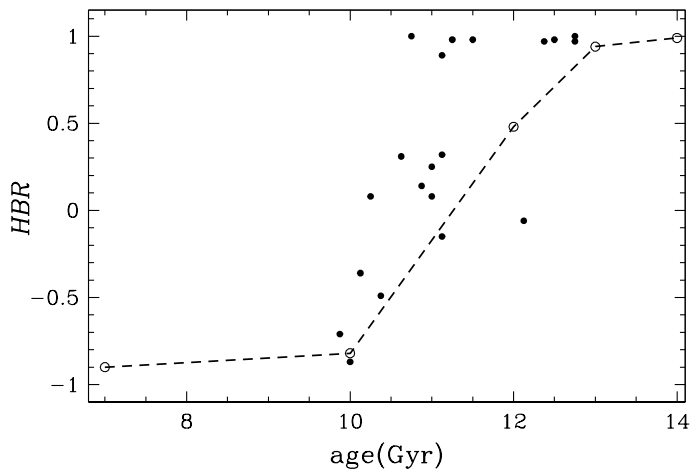


Fig. 4. The relationship between the age and the HB morphology parameter, HBR , in GCs. The solid circles are the selected GCs in our Galaxy, which are in the metallicity range of $-1.6 < [Fe/H] < -1.1$. The open circles denote our model calculations in Fig.2, which from left to right correspond to cluster ages of 7, 10, 12, 13 and 14 Gyr, respectively.

GCs in our Galaxy and the parameter, HBR , which is used to describe the HB morphology of GCs (Lee et al. 1990; Lee et al. 1994). The parameter, HBR , is defined as follows,

$$HBR = (B - R)/(B + V + R), \quad (3)$$

where B, V, R have the same meaning as described in Section 3.2. The value of the parameter, HBR , is in the range of -1 to 1. The value of -1 means that all HB stars settle on red HB; on the other hand, the value of 1 means that GC presents a whole blue HB. Therefore, the larger of the HBR parameter, the bluer of the HB morphology in GCs. The values of HBR parameter for GCs in Fig.4 are from the catalogue of Harris (1996), and the age of GCs used in this figure is from Gratton et al. (2010)². To compare the observation with our results, we just choose the GCs in the metallicity range of $-1.6 < [Fe/H] < -1.1$ in Fig.4, which is around the metallicity used in Fig.2 (i.e., $Z = 0.001$ or $[Fe/H] = -1.3$). This limit weakens the effect of metallicity on HB morphology, thus the effect of age on HB morphology could be revealed more clearly. In Fig.4, the selected GCs are denoted by solid circles, and our model calculations in Fig.2 are denoted by open circles, for which the ages from left to right are 7, 10, 12, 13 and 14 Gyr, respectively.

One can see in Fig.4 that, for the selected GCs in our Galaxy, the value of HBR increases with the increasing age of the GCs, which means the HB morphology becomes bluer when the ages of the GCs become older. This result is consistent with the one obtained from Fig.2, and also can be seen clearly from the dashed line in Fig.4. However, for a fixed age of GCs, our synthetic HB produced by tidally enhanced stellar wind in Fig.4 is a little redder than the observed ones. This may be due to **the fact** that we do not consider the **common envelope (CE) and Roche lobe over flow (RLOF)** processes in binary evolution for our calculations (see Section 3.1 and Paper I). These processes can produce EHB stars (Han et al. 2002, 2003), and thus make HB bluer.

² The relative ages of GCs in Gratton et al. (2010) are from Marin-Franch et al. (2009) and De Angeli et al. (2005).

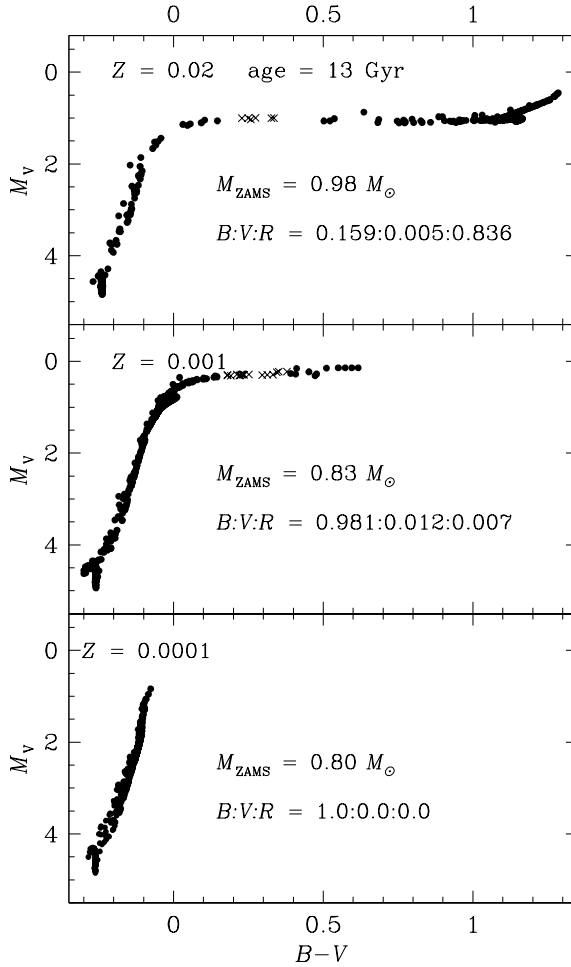


Fig. 5. Same as Fig.1, but with a higher binary fraction of 80% rather than 50%.

We also adopted different value of Reimers mass-loss efficiency (e.g., $\eta=0.25$, which is the value we used in Paper I) in our model calculations. We found that, for $\eta=0.25$, the result is similar with that in Fig.4. However, to produce a blue HB morphology (e.g., $HBR \gtrsim 0.5$), the age of GCs should be larger than 15 Gyr. This indicates that $\eta=0.25$ is too small to produce the observed HB morphology in GCs. Renzini & Fusi Pecci (1988) demonstrated that observed HB morphologies in GCs with $Z \approx 0.001$ demand $\eta = 0.4 \pm 0.04$. That is why we use the value of $\eta = 0.45$ in this paper, but it does not influence our results obtained in Paper I, since we can obtain the same results using a little smaller age of GCs for a larger value of η .

4.3. Effects of binary fraction on HB morphology

In our model calculations, all stars are in binary systems, but the binaries with long orbital periods are actually single stars. The separation distribution of binary systems described in Section 2.3 implies that about 50% of binary systems have their orbital periods shorter than 100 yr. To investigate the effects of binary fractions on our final results, we also adopted

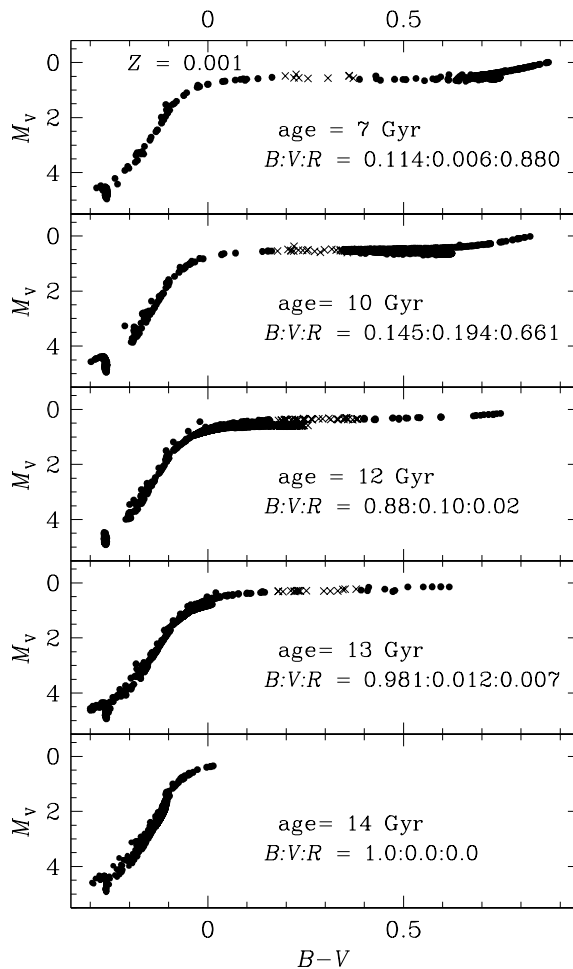


Fig. 6. Same as Fig.2, but with a higher binary fraction of 80% rather than 50%.

various binary fractions in our calculations (i.e., 10%, 15%, 20%, 30% and 80%)³. The result of model calculation for a binary fraction of 80% is shown in Fig.5 and Fig.6. The input parameters in Fig.5 and Fig.6 are the same as in Fig.1 and Fig.2 respectively, except for the binary fraction.

By comparing Fig.5 and Fig.1, one can see that, with the binary fraction increasing, the number ratio of HB stars bluer than the RR Lyrae instability strip increases, while the number ratio of red HB stars decreases (e.g., in the top panel of Fig.5, the number ratio of HB stars bluer than RR Lyrae instability strip is 15.9%, as opposed to 4.5% in top panel of Fig.1; while the number ratio of red HB stars is 83.6%, versus 95.4% in top panel of Fig.1). We can also obtain this result by comparing Fig.6 and Fig.2 (note that the model calculations for binary fraction of 10%, 15%, 20% and 30% show similar results). This is due to the fact that the orbital period in which tidally enhanced stellar wind significantly affects mass loss of the primary star is from $\log P/\text{day} \approx 3.1$ to $\log P/\text{day} \approx 3.5$ (see Table 2 and Table 3), and the orbital periods of binaries in this range are less than 100 yr. Therefore, for a given total number of

³ All these binary fractions are for the binary systems which have their orbital periods less than 100 yr.

binary samples, when the fraction of binary systems with their binary orbital periods less than 100 yr increases, more primary stars will be influenced by tidally enhanced stellar wind, and then more blue and extreme HB stars will be produced.

This result indicates that higher binary fraction may make the HB morphology become bluer, which implies that binary population is a possible second parameter candidate. However, Milone et al. (2012) estimate the binary fraction for 59 Galactic GCs by analyzing the number of stars located on the red side of the main-sequence fiducial line (also see Sollima et al. 2007). Moreover, they studied the relationship between the binary fraction and the HB morphology parameters, and concluded that there is small or null impact of binary populations on HB morphology (see Fig.47 and Section 5.6.3 in their paper). At first glance, their results contradict with us. However, the sample GCs in Milone et al. (2012) have different metallicities and ages, which are very important parameters affecting HB morphology in GCs (Gratton et al. 2010; Dotter et al. 2010). Therefore, Milone et al. (2012) did not remove the effects of metallicity and age on HB morphology when studying the effects of binary fraction on HB morphology, and it will significantly influence the final results ⁴. On the other hand, our result that higher binary fraction may make HB morphology become bluer is obtained by comparing GCs with fixed metallicity and age but different binary fractions. This means that we removed the effects of metallicity and age when studying the effects of binary fraction on HB morphology. Thus, the results obtained by Milone et al. (2012) can not exclude binary populations as a second parameter candidate which may affect HB morphology in GCs.

One can also see that, though the binary fraction is higher than that of Fig.1, the synthetic HB for $Z=0.02$ in top panel of Fig.5 still presents a distinct gap between red and blue HB, with very few of HB stars located in RR Lyrae instability strip (similar results are obtained for other different binary fractions). This result indicates that binary fraction may have little effects on bimodality of HB, and the bimodality on HB may mainly depend on metallicity of GCs (see our discussion in Section 4.1).

5. Conclusions

In this paper, under the consideration of tidally enhanced stellar wind during binary evolution, we studied the effects on the HB morphology of GCs with different metallicities and ages. We found that metal-poor GCs should present more bluer HB morphology than the metal-rich ones which is consistent with previous work. Furthermore, we found in our calculations that the envelope-mass distributions of ZAHB stars produced by tidally enhanced stellar wind are very similar for different metallicities. However, the synthetic HB for $Z=0.02$ produced by tidally enhanced stellar wind presents a distinct gap between red and blue HB, while this feature is not seen clearly in the synthetic HB for $Z=0.001$ and 0.0001 . We also found that old GCs present more bluer HB than the young ones, **which is also consistent with previous work**. We compared our results with the observation in the age-*HBR* diagram of GCs. **Furthermore, we studied the effects of binary**

⁴ For example, we used a binary fraction of 10% in calculation and found that, though the binary fraction is relatively low, the synthetic HB for $Z=0.0001$ at 13 Gyr is still a pure blue HB (e.g., $HBR=1$). It means that effects of metallicity may cover the effects of binary fraction on HB morphology at very low metallicity.

fraction on our final results, and found that higher binary fraction may make HB morphology become bluer. We finally discussed our results with recent observations.

Acknowledgements. We thank the anonymous referee for his/her valuable comments and suggestions that helped us to improve the paper. This work is supported by the National Natural Science Foundation of China (Grant Nos.11033008, 10973036, 11173055, 11203065 and 11273053) and the Chinese Academy of Sciences (Grant No. KJCX2-YW-T24).

References

- Buonanno, R., Corsi, C., Bellazzini, M., Ferraro, F. R., & Fusi Pecci, F. 1997, *ApJ*, 113, 706
- Carretta, E., Bragaglia, A., Gratton, R. G.; et al. 2010, *A&A*, 516, A55**
- Catelan, M. 2009, *Ap&SS*, 320, 261
- Chaboyer, B., Green, E. M., & Liebert, J. 1999, *AJ*, 117, 1360
- Chen, X. F., & Tout, C. A. 2007, *Chinese J. Astron. Astrophys.*, 7, 245
- Dalessandro, E., Salaris, M., Ferraro, F. R., et al. 2011, *MNRAS*, 410, 694**
- D'Antona, F., Bellazzini, M., Caloi, V., Fusi Pecci, F., Galletti, S., & Rood, R. T. 2005, *ApJ*, 631, 868
- D'Antona, F., & Caloi, V. 2004, *ApJ*, 611, 871
- D'Antona, F., & Caloi, V. 2008, *MNRAS*, 390, 693
- D'Antona, F., Caloi, V., Montalbán, J., Ventura, P., & Gratton, R. 2002, *A&A*, 395, 69
- De Angeli, F., Piotto, G., Cassisi, S. et al. 2005, *AJ*, 130, 116
- Dotter, A., Sarajedini, A., Anderson, J., et al. 2010, *ApJ*, 708, 698**
- Dupree, A. K., Smith, G. H., Strader, J., et al. 2009, *AJ*, 138, 1485.
- Eggleton, P. P. 1971, *MNRAS*, 151, 351
- Eggleton, P. P. 1972, *MNRAS*, 156, 361
- Eggleton, P. P. 1973, *MNRAS*, 163, 279
- Friel, E. D., & Janes, K. A. 1993, *A&A*, 267, 75
- Fusi Pecci, F., Ferraro, F. R., Bellazzini, M., Djorgovski, S., Piotto, G., & Buonanno, R. 1993, *AJ*, 105, 1145
- Gratton, R. G., Carretta, E., & Bragaglia, A., 2012, *A&A Rev.*, 20, 50**
- Gratton, R. G., Carretta, E., Bragaglia, A., et al. 2010, *A&A*, 517, A81**
- Han, Z., Podsiadlowski, P., & Eggleton, P. P. 1994, *MNRAS*, 270, 121
- Han, Z., Podsiadlowski, P., Maxted, P. F. L., Marsh, T. R., & Ivanova, N. 2002, *MNRAS*, 336, 449
- Han, Z., Podsiadlowski, P., Maxted, P. F. L., & Marsh, T. R. 2003, *MNRAS*, 341, 669
- Harris, W. E. 1996, *AJ*, 112, 1487
- Kaluzny, J., & Rucinski, S. M. 1995, *A&AS*, 114, 1
- Kaluzny, J., & Udalski, A. 1992, *Acta Astron.*, 42, 29
- Koopmann, R. A., Lee, Y. W., Demarque, P., et al. 1994, *ApJ*, 423, 380
- Lee, H. C., Yoon, S. J., & Lee, Y. W. 2000, *AJ*, 120, 998**
- Lee, Y. W., Demarque, P., & Zinn, R. 1990, *ApJ*, 350, 155
- Lee, Y. W., Demarque, P., & Zinn, R. 1994, *ApJ*, 423, 248
- Lei, Z., Chen, X., Zhang, F., & Han, Z. 2013, *A&A*, 549, A145
- Lejeune, T., Cuisinier, F., & Buser R. 1997, *A&AS*, 125, 229
- Lejeune, T., Cuisinier, F., & Buser R. 1998, *A&AS*, 130, 65
- Liebert, J., Saffer, R. A., & Green, E. M. 1994, *AJ*, 107, 1408
- Marin-Franch, A., Aparicio, A., & Piotto, G., et al. 2009, *ApJ*, 694, 1498
- Milone, A. P., Piotto, G., Bedin, L. R., et al. 2012, *A&A*, 540, A16**
- Moehler, S. 2010, *MmSAI*, 81,838
- Paxton, B., Bildsten, L., Dotter, A., et al. 2011, *ApJS*, 192, 3
- Percival, S. M., & Salaris, M. 2011, *MNRAS*, 412, 2445**
- Peterson, R. C., & Green, E. M. 1998, *ApJ*, 502, L39
- Piotto, G., Bedin, L. R., Anderson, J., et al. 2007, *ApJ*, 661, L53**
- Piotto, G.; Milone, A. P.; Anderson, J.; et al. 2012, *ApJ*, 760, 39**
- Pols, O. R., Schröder, K. P., Hurley, J. P., et al. 1998, *MNRAS*, 298, 525

- Pols, O. R., Tout, C. A., Eggleton, P. P., & Han, Z. 1995, *MNRAS*, 274, 964
- Pols, O. R., Tout, C. A., Schröder, K. P., et al. 1997, *MNRAS*, 289, 869
- Recio-Blanco, A., Aparicio, A., Piotto, G., De Angeli, F., & Djorgovski, s. G. 2006, *A&A*, 452, 875
- Reimers, D. 1975, *MSRSL*, 8, 369
- Renzini, A., & Fusi Pecci, F. 1988, *ARA&A*, 26, 245
- Rood, R. T. 1973, *ApJ*, 184, 815**
- Sandage, A., & Wallerstein, G. 1960, *ApJ*, 131, 598
- Soker, N. 1998, *AJ*, 116, 1308
- Soker, N., & Hadar, R. 2001, *MNRAS*, 324, 213
- Soker, N., & Harpaz, A. 2000, *MNRAS*, 317, 861
- Soker, N., & Harpaz, A. 2007, *ApJ*, 660, 699
- Sollima, A., Beccari, G., Ferraro, F. R., et al. 2007, *MNRAS*, 380, 781**
- Sweigart, A. V. 1997, *ApJ*, 474, L23
- Tout, C. A., & Eggleton, P. P. 1988, *MNRAS*, 231, 823
- Willson, L. A. 2000, *ARA&A*, 38, 573